Reply to reviewer #2:

The authors conducted extensive field observations of flow, hydrographic conditions and the concentration of biogeochemical substances over the shelf and slope off Peru. They combined the satellite remote-sensed SLA and SST and the field observations to investigate the causes of the intra-seasonal variabilities of, for example, DO in the water column and qualitatively discussed the characteristics of the propagating CTW, and those of the variant types of nutrients and DO, as well as oscillation in OMZ. This manuscript is extensively condensed and improved from its previous OSD version with great improvement in the scientific focus. This manuscript is well-written, and the reflected sciences are well presented. I thereafter intend to suggest an "minor revision". However, since I still have serval suggestions for the authors to consider, I thereby suggest a major revision to let the authors think more in depth into the dynamics they proposed.

We kindly thank the reviewer for the reevaluation of our manuscript.

In the manuscript we have improved the discussion of our results by focusing on our data and by adding a schematic of oxygen and nutrient changes. In the introduction we have reduced the number of cited studies and section 4.4 was reworked. We have improved the discussion as well by focusing on our own results. Additionally, we have checked the whole manuscript for typos and wrong numbering.

In our detailed response below, comments by the reviewer are in bold letters and changes in the manuscript are expressed in italic letter.

1) The authors revised the manuscript from their last submission to the OSD journal, and there are typos left. I suggest the authors to go through the entire manuscript very carefully.

We thank you for pointing us at these issues, we made sure to check the manuscript for such typos.

For example, L265, the last "maintaining" should be "maintain".

Changed accordingly.

L280, 6 month should be "months".

Changed accordingly.

L305, what does this "not inconsistent" mean? "consistent"? I didn't see any verb in this sentence.

We agree that this sentence is not well written and reformulated it. Now we use "agrees" instead of the for statement "not inconsistent".

Along the equator, the propagation speed of the SLA is about 2.7 m s^{-1} (dashed line in the left panel of Fig. 7) which agrees with the phase speed of a first vertical mode equatorial Kelvin waves (e.g. Yu and McPhaden, 1999).

I stop here, but it is the duty of the authors to check the expressions sentence by sentence.
2) Too many citations in the introduction section. I suggest you to just preserve the most representative ones, and reduce the number of references substantially. Obviously, you didn't discuss all those studies.

Thank you very much for this suggestion, accordingly we went through our introduction and restricted the citations to the most important ones for each statement.

And I can not find Winkler 1888 (L130)?

The publication by Winkler (1888) may be found using the doi-number included in the references (dx.doi.org/10.1002/cber.188802102122). Indeed, neither Web of Science nor Google Scholar find the article when searching for the title.

3) L190, what does the exact meaning of the long sentences starting with "The data were …" I can understand that you did spatial smoothing but the description here is very confusing.

We agree with you that this sentence is very long and therefore confusing, we have decided to shorten this sentence and restrict it to the most important information that smoothing was applied.

Smoothed hydrographic and biogeochemical properties along the 12° S section were calculated by interpolating the data vertically onto common potential density surfaces. Averaging in density space removes the effect of signal smearing due to vertical displacement caused by internal waves. The profiles were then averaged in bins of 2 km according to distance from the coastline and then smoothed using 2-D Gaussian weights. In a final step, the averaged and smoothed sections were vertically transformed back into depth space using the smoothed depth – density relation.

4) You clarified the respective roles of wind stress curl and wind stress itself. In section 4.2.1. This is good, but could you please also show in the response (you may don't want to include them into the revised manuscript) about the role of tides? You don't need to discuss the flood-ebb tides, but spring-neap tides may play some roles?

From mooring data of velocity collected in early 2013 at the same location we have calculated the alongshore amplitudes and phases of the O1, K1, N2, M2, S2 tidal constituents. From these we have reconstructed a 30 day timeseries of the alongshore velocities caused by the tides (Fig. 1).
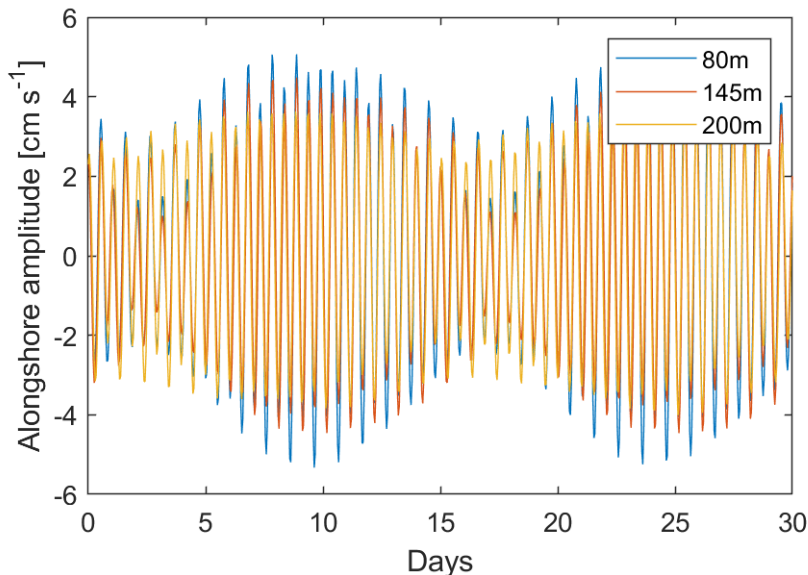

Figure 1: Tidal alongshore velocities at three different water depths at the 12° S section off Peru.

The tides may introduce velocities of up to 5 cm s^{-1} and the difference between neap and spring tide amplitude is about 2 cm s^{-1}. These velocities are small compared to the increase of poleward flow of more than 20 cm s^{-1} over a large part of the PCUC depth range and therefore very unlikely to be important for the changes of PCUC strength.

5) Still, section 4.4 is too descriptive. This is important, since that massive and systematic observations are new to us to understand the background and variabilities. However, it is still your obligation to help the readers to get insight into your science.

According to your suggestion we have improved section 4.4 to explain better explain the concentration patterns of the nutrients and which biogeochemical processes are responsible for them. Overall, we made this section much less descriptive and connect changes of different parameters with each other more.

Please find the changed section 4.4 in the revised manuscript.

I thereby strongly suggest the authors to include a schematic plot for different patterns of the CTWs propagation, changes in the shelf currents and the responses of the nutrients and DO you show in section 5.

Following your suggestion, we have included a schematic of the oxygen and nutrient response to the circulation change.
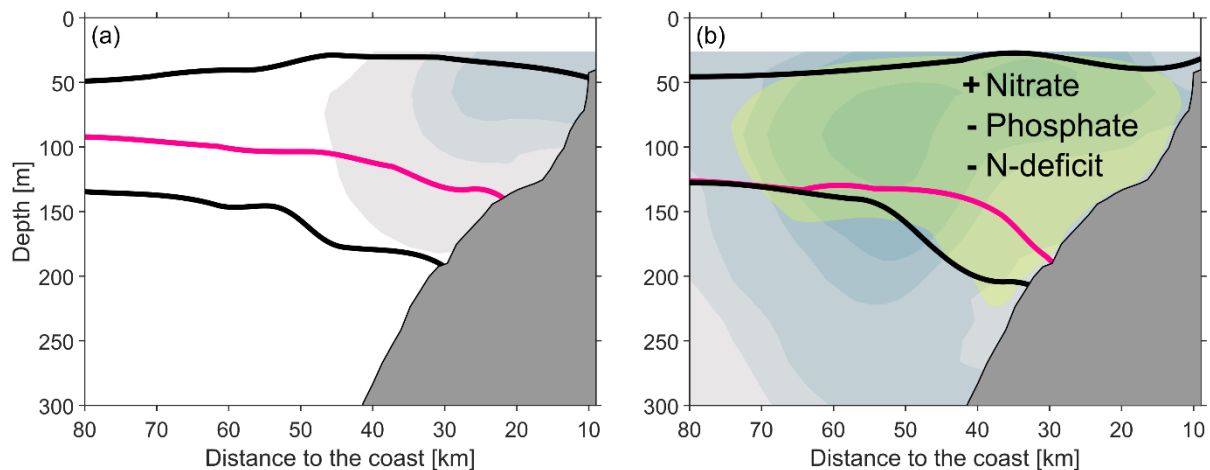

Figure 12: Schematic of the conditions off Peru during the initial phase of weak PCUC flow (a) and strong PCUC flow (b). Alongshore circulation is shown as colour shading, two isopycnals are sown in black and the top of the anoxic zone in magenta (represented by the 2 µmol kg^{-1} isoline). The green shaded area in (b) shows the region of increased nitrate, decreased phosphate concentrations and decreased nitrogen deficit.

You cited too much of some others studies in the section 5, and some contents can be extracted from your own observation. I may suggest you to further condense and deepen the sciences in section 5 by your own data, although the current arrangement of logics looks sensible. This is the core of my major concern.

In the discussion (section 5) we focus more on our results and include the aforementioned schematic for this as well. Additionally, we have removed parts of the discussion which were not directly focused on the results of our study but relying on a lot of cited literature.

Please find the changed section 5 in the revised manuscript.

Reply to reviewer #3

I read the revised manuscript and the authors' responses to the comments. Overall, following both reviewers' comments, the authors have made adequate modifications to the deficiencies, especially the unclear explanation on physical processes, in the first draft. The revised paper have discussed the possible effects of various dynamic factors, including CTWs, local winds, topography, eddies etc., on the intraseasonal strengthening of PCUC. The comprehensive analyses of these potential factors indicate the essential role of CTWs in modulating the variability of sea level and PCUC. Although the authors has not carried out further numerical simulation, the existing data analysis results still provide a lot of valuable information on dynamic processes and physical-biogeochemical interactions. These interesting results are worthy of further quantification through the numerical experiments of coupling models in the future. At the same time, I also noticed that some new errors were introduced during the modification. Thus, I suggest that the authors read through the text and revise it carefully.

We thank you very much for reviewing our manuscript.

In the manuscript we have improved the discussion of our results by focusing on our data and by adding a schematic of oxygen and nutrient changes. In the introduction we have reduced the number of cited studies and section 4.4 was reworked. We have improved the discussion as well by focusing on our own results. Additionally, we have checked the whole manuscript for typos and wrong numbering.

In our detailed response below, comments by the reviewer are in bold letters and changes in the manuscript are expressed in italic letter.

Detailed comments are the following:

1) The authors modified the order of some figures, but the text part was not completely revised accordingly. As a result, some figures do not match the corresponding discussions in the text. For example: l 284-288: Fig. 7 should be Fig. 6. The descriptions of Figures 8, 9 and 10 in Sections 4.3-4.4 actually correspond to figures 9, 10 and 11 in the list.

We thank you for noting this and have corrected the figure referencing.

2) Section 4.1.3 should be Section 4.2.3.

Thank you very much for finding this mistake, we have changed the section numbering.

3) P7, L272-274: "…… However, during the later period the strong acceleration of the poleward flow occurred, requiring an intensification of alongshore wind stress." It is difficult to imagine why the intensification of alongshore wind will accelerate the poleward undercurrent. To my understanding, given that the prevailing winds are southeasterly along the Peruvian coast, the weakening of local southeast trade winds will excite poleward-propagating downwelling CTWs, similar to those driven by the equatorial westerly winds. In fact, some studies on the coastal El Nino in spring 2017 have shown that the northerly coastal wind anomalies and the equatorial westerly winds anomalies are both important in maintaining the high sea level along the Peruvian coast (e.g. Peng et al., 2019).
Peng, Q., Xie, S., Wang, D. et al. Coupled ocean-atmosphere dynamics of the 2017 extreme coastal El Niño. Nat Commun 10, 298 (2019). https://doi.org/10.1038/s41467-018-08258-8.

Indeed, this formulation is difficult to understand. An increase of alongshore wind stress will create upwelling waves reducing poleward transport, but this effect vanishes once the wave propagated poleward. Additionally, these waves set up an alongshore pressure gradient which is forcing the PCUC and persists until the wind forcing changes (Yoon and Philander, 1982).

We have changed the paragraph to be shorter and focus on the mismatch of wind stress and poleward flow which is therefore not the driven of PUC intensification. Therefore, we have removed the complicated and easily misunderstood explanation of the mechanisms of wind forcing from this section.

On May 15 the wind stress increased and remained elevated for a period of about 5 days. This is not in agreement with the changes of poleward transport: The transport increased from late April to its maximum mid-May, whereas the alongshore wind stress in this period did first decrease and later increase.

In the discussion we have included the study of Peng et al. when discussing the role of CTWs for the warming during the Coastal El Niño.

References:

Yoon, J.-H. and Philander, S. G. H.: The generation of coastal undercurrents, J. Oceanogr. Soc. Jpn., 38(4), 215–224, doi:10.1007/bf02111104, 1982.

Influence of intraseasonal eastern boundary circulation variability on hydrography and biogeochemistry off Peru

Jan Lüdke[1], Marcus Dengler[1], Stefan Sommer[1], David Clemens[1], Sören Thomsen[2], Gerd Krahmann[1], Andrew W. Dale[1], Eric P. Achterberg[1,3], Martin Visbeck[1,3]

[1]GEOMAR Helmholtz Centre for Ocean Research Kiel, Düsternbrooker Weg 20, D-24105 Kiel, Germany

[2]LOCEAN-IPSL, IRD/CNRS/Sorbonnes Universites (UPMC)/MNHN, UMR 7159, Paris, France

[3]Kiel University, Kiel, Germany

Correspondence to: Jan Lüdke (jluedke@geomar.de)

Abstract. ~~The Peruvian upwelling system is characterized by high primary productivity fuelled by the supply of nutrients in a highly dynamic boundary circulation. The intraseasonal evolution of the physical and biogeochemical properties is analysed based on shipboard observations conducted between April and June 2017 off central Peru and remote sensing data. The poleward transport in the subsurface Peru Chile Undercurrent was highly variable and strongly intensified between mid and end of May. This intensification was likely caused by a first baroclinic mode coastal trapped wave excited at the equator at about 95° W that propagated poleward along the South American coast. An intensified poleward flow increases water mass advection from the equatorial current system to the study site. The impact of the elevated advection was mostly noticed in the nitrogen cycle. Shorter transit times between the equator and the coast off central Peru led to a strong increase in nitrate concentrations, less fixed nitrogen loss to N$_2$, and a decrease in the nitrogen deficit. The study highlights the importance of alongshore advection due to coastal trapped waves for the nutrient budget and the cumulative strength of N-cycling in the Peruvian OMZ.~~

The intraseasonal evolution of physical and biogeochemical properties during a coastal trapped wave event off central Peru is analysed using data from an extensive shipboard observational programme conducted between April and June 2017, and remote sensing data. The poleward velocities in the Peru Chile Undercurrent were highly variable and strongly intensified to above 0.5 m s^{-1} between mid and end of May. This intensification was likely caused by a first baroclinic mode downwelling coastal trapped wave, excited by a westerly wind anomaly at the equator at about 95° W. Local winds along the South American coast did not impact the wave. Although there is general agreement between the observed cross-shore-depth velocity structure of the coastal trapped wave and the velocity structure of first vertical mode solution of a linear wave model, there are differences in the details of the two flow distributions. The enhanced poleward flow increased water mass advection from the equatorial current system to the study site. The resulting shorter alongshore transit times between the equator and the coast off central Peru led to a strong increase in nitrate concentrations, less anoxic water, likely less fixed nitrogen loss to N$_2$, and a decrease of the nitrogen deficit compared to the situation before the poleward flow intensification. This study highlights the role of changes in the alongshore advection due to coastal trapped waves for the nutrient budget and the cumulative strength of N-cycling in the Peruvian oxygen minimum zone. Enhanced availability of nitrate may impact a range of pelagic and benthic elemental cycles, as it represents a major electron acceptor for organic carbon degradation during denitrification and is involved in sulfide oxidation in sediments.

1 Introduction

The Peruvian Upwelling System (PUS) is one of the ~~biologically~~ most productive regions in the world's ocean ~~resulting in~~with economically important fish catches (e.g. Carr, 2002; Chavez et al., 2008). Located in the Eastern Tropical South Pacific (ETSP), the high surface productivity of the PUS is most pronounced within a 100 km ~~of~~wide stretch along the Peruvian coast between 4° and 16° S (Pennington et al., 2006). Equatorward winds favour upwelling throughout the year (Bakun and Nelson, 1991; Strub et al., 1998) and enable a supply of nutrients from subsurface waters and benthic boundary layer to the euphotic zone, stimulating high primary productivity (Pennington et al., 2006). ~~Beneath~~Below the ~~upwelling system, the~~surface layer, low oxygen waters supplied to the PUS and enhanced local oxygen consumption due to remineralization of exported organic matter lead to the development of a pronounced Oxygen Minimum Zone (OMZ). The core of the OMZ with upper and lower bounds at about 30 – 200 m and 400 – 500 m depth, respectively, is considered to be ~~fully~~functionally anoxic (e.g. Ulloa et al., 2012, Thomsen et al. 2016).

The eastern boundary circulation in the PUS is dominated by the poleward Peru-Chile Undercurrent (PCUC) occupying the upper continental slope and shelf at depths from 50 to 200 m (Fig. 1, e.g. Gunter, 1936; Chaigneau et al., 2013). It carries low-oxygen and high-nutrient Equatorial Subsurface Waters (ESSW), which constitutes the main source of the ~~coastal~~upwelled waters (~~Brink et al., 1983; Penven et al., 2005;~~ Silva et al., 2009; Albert et al., 2010~~; Chaigneau et al., 2013; Grados et al., 2018~~). Mean poleward velocities associated with the PCUC are between 0.05 and 0.15 ms^{-1} (Chaigneau et al., 2013). The origin of its source waters is still under debate. Chaigneau et al~~.~~., (2013) traced its source waters to the Equatorial Undercurrent supplying the PCUC via the Ecuador-Peru Coastal Current ~~which~~, that flows poleward along the coast between the equator and 5° S. In contrast, a regional model analysis by Montes et al. (2010) suggests that the source waters of the PCUC originate predominately from the eastward Southern Subsurface Countercurrents, flowing south of the equator (Fig. 1). Above the PCUC, upwelling dynamics imply the existence of an equatorward geostrophic surface jet, known as the Peru Coastal Current (e.g. Hill et al., 1998; Kämpf and Chapman, 2016). Additional features of the eastern boundary circulation are the Peru-Chile Current flowing equatorward offshore of the PCUC, and the Chile-Peru Deep Coastal Current flowing equatorward below the PCUC (Fig. 1, Strub et al., 1998; ~~Penven et al., 2005; Czeschel et al., 2011;~~ Chaigneau et al., 2013).

The PUS exhibits variability on a wide range of timescales, including intraseasonal (e.g. ~~Brink et al., 1982;~~ Gutiérrez et al., 2008; ~~Belmadani et al., 2012; Pietri et al., 2014,~~ Illig et al., 2018a, 2018b), seasonal (e.g. Pizarro et al., 2002~~; Chaigneau et al., 2013~~), and interannual to decadal (~~Pizarro et al., 2002; Ramos et al., 2008;~~ e.g. Graco et al., 2017). ~~In particular, intraseasonal~~Intraseasonal variability of oxygen and nutrient ~~concentration~~concentrations along the Peruvian ~~continental slope and on the shelf~~margin are known to strongly impact pelagic and benthic ~~and pelagic~~ ecosystems within the OMZ and the upwelling region above (e.g. Gutiérrez et al., 2008; Echevin et al., 2014; Graco et al., 2017). ~~A prominent benthic example is the biota responses to the frequency of oxygenation episodes changing from macro invertebrates dominated biomass to bacterial mats (Thioploca) or when the frequency reduces (e.g. Gutiérrez et al., 2008). Furthermore, the availability of nitrate nutrients in the anoxic waters of the OMZ allows for degradation of organic matter and is thereby consumed, while the lack of nitrate nutrients favours benthic sulfide emissions and sulfide plumes in the water column (e.g. Dale et al., 2016; Schunck et al., 2013).~~

A key ~~process~~factor thought to be responsible for the intraseasonal variability of ~~the solute~~oxygen and nutrient concentrations is the variability of the eastern boundary circulation~~. Intraseasonal variability of the eastern boundary circulation is either,~~ forced locally by changes of the wind system above the PUS or forced remotely by variability of the wind system at the equator. Strengthening (weakening) of the local alongshore winds causes intensified (reduced) Ekman divergence close to the coast that accelerates (decelerates) the coastal surface jet (e.g. Philander and ~~Yonn~~Yoon, 1982; ~~Yoon and Philander, 1982; McCreary et al., 1987;~~ Fennel et al., 2012). ~~At the same time,~~ Coastal Trapped Waves (CTWs) are excited ~~propagating~~and propagate poleward to set up an alongshore pressure gradient balancing ~~the~~an accelerating (decelerating) alongshore flow (Yoon and Philander, 1982). Due to differences in vertical structure of the surface jet and the excited CTWs, the poleward flowing PCUC

accelerates (decelerates). ~~Likewise, variability of local wind stress curl forces variability of the poleward undercurrent through enhancing or reducing Sverdrup transport in the eastern boundary current regime (e.g. McCreary and Chao, 1985; Marchesiello et al., 2003; Junker et al., 2015; Klenz et al., 2018). Local wind forced variability of eastern boundary poleward undercurrents have been reported from all eastern boundary upwelling regions on time scales from intraseasonal to seasonal (e.g. Allen and Smith, 1981;~~Furthermore, variability of local wind stress curl forces variability of the poleward undercurrent by affecting the magnitude of Sverdrup transport in the eastern boundary current regime (e.g. McCreary and Chao, 1985; Klenz et al., 2018). Variability of local wind stress curl forces also variability of time scales from intra-seasonal to seasonal (e.g. Marchesiello et al., 2003, Junker et al., 2015, Klenz et al., 2018).

Alternatively, ~~intraseasonal~~ variability ~~of the eastern boundary circulation in the PUS may be of equatorial origin and manifested as a poleward-moving CTW as well. Variability~~ of zonal winds in the equatorial Pacific forces equatorial Kelvin waves that propagate eastward. Upon reaching the continental margin, part of their incoming energy is transmitted poleward along the southwestern coast of South America as CTWs (e.g. Moore and Philander, 1977; Enfield et al., 1987~~; Rydbeck et al., 2019)~~). Early measurement programs off Peru investigating intraseasonal alongshore current variability showed coherent CTW signals with periods of 5-50 days propagating poleward between 5° S and 15° S (Brink et al., 1980, 1983; Romea and Smith, 1983). Tide gauge data and ~~the~~a lack of correlated local winds suggested that the CTWs were predominately of equatorial origin. Similarly, intraseasonal CTW variability (50-day period) in the PCUC off Chile ~~having~~with velocity amplitudes of up to 0.7 m s^{-1} were shown to have originated from wind variability in the central equatorial Pacific (Shaffer et al., 1997). Modelling efforts confirm that equatorially- forced intraseasonal CTWs propagate along the eastern South American coast to as far as 30° S (Hormazabal et al., 2002; Illig et al., 2018b).

~~While modulating the alongshore circulation and vertical velocities, poleward~~Poleward propagating CTWs produce vertical displacements of the pycnocline of the order of tens of meters and sea level changes of a few centimeters (Leth and Middelton, 2006; ~~Colas et al., 2008;~~ Belmadani et al., 2012). They also modulate the alongshore circulation, that is, CTWs that have a positive sea level anomaly and a downward displacement of the thermocline (downwelling waves) exhibit poleward flow while CTW that have a negative sea level anomaly (upwelling waves) exhibit equatorward flow (e.g. Echevin et al., 2014). The combined effect alters the horizontal and vertical supply of nutrients in the PUS. Modelling ~~efforts~~ and satellite observations suggest that subsurface nutrient and chlorophyll intraseasonal variability in the PUS are mainly forced by remotely forced CTWs (Echevin et al., 2014). The simulations indicate that the shoaling and deepening of the nutricline, as well as the horizontal currents associated with the CTW, induce a nutrient flux in and out of the euphotic layer, which impacts primary production. On the other hand, intraseasonal sea surface temperature (SST) variability is suggested to be mainly driven by local winds and heat fluxes ~~while~~with CTWs ~~play~~playing only a minor role (Dewitte et al., 2011; Illig et al., 2014). ~~On interannual timescales~~Variability of CTWs can ~~dominate the variability in~~affect hence nutrient concentrations ~~(Graco et al., 2017)~~ and bottom water oxygen levels ~~that can lead to strong~~(Graco et al., 2017) on intra-seasonal but also inter-annual timescales. The benthic biota reacts strongly to periods of oxygenation or deoxygenation, which are caused by CTWs, and the dominant benthic community changes ~~in benthic ecosystems (Gutierrez~~from macro-invertebrates to bacterial mats (*Thioploca/Beggiatoa*) after prolonged low-oxygen conditions (Gutiérrez et al., 2008~~).~~) and benthic sulfide emissions and toxic sulfide plumes in the water column can occur (Schunck et al., 2013; Dale et al., 2016).

Here, we use an extensive multi-parameter data set from a multi-cruise observational program to analyse the impact of a strongly elevated and individual propagating CTW on the circulation, hydrography and nutrient concentrations in the PUS. By visiting sampling stations several times over a period of more than two months, we measured the variability of the circulation and hydrographic and biogeochemical conditions almost continuously and can distinguish the intraseasonal variability from ~~that~~processes taking place on shorter time scales ~~due to other processes~~.

The conditions off Peru in early 2017 were further affected by anomalously warm temperatures in the upper ocean during
120   March associated with a coastal El Niño event (e.g. Garreaud, 2018; Echevin et al., 2018). Our observations ~~on which this analysis is based~~ cover the declining phase of the coastal El Niño event in April and May when SST anomalies were decreasing.

2 Data

2.1 Ship data

Within the framework of the Collaborative Research Center 754 "Climate-~~biogeochemistry interactions~~Biogeochemistry
125   Interactions in the ~~tropical ocean~~Tropical Ocean", we carried out a combined physical and biogeochemical sampling program
in the ETSP from April to June 2017 during several legs on R/V Meteor (Tab. 1). A regional focus during the four individual
cruises of the sampling program was a transect starting at shallow waters off Callao (Peru) at about 12° S running offshore
perpendicular to the coastline ~~to~~and ends at water depths ~~larger~~greater than 5000 m and ~~>~~more than 100 km offshore (Fig. 1).
During the first R/V Meteor cruise M135, the 12° S section was studied ~~at~~towards the end of the cruise ~~on~~ (April 7 ~~–~~ 8~~.~~).The
130   two subsequent cruises M136 and M137 focused on benthic and pelagic work off Peru between 11° and 14° S (~~Sommer et al., 2019,~~ Dengler and Sommer, 2019; Sommer et al., 2019). Benthic lander measurements required the vessel to remain close to
the section between April 18 and May 29, 2017, when repeated hydrographic and velocity measurements along the section
were collected. The section was again ~~resampled~~sampled during the final cruise M138 ~~on~~ (June 24~~.~~). In this study, we analyse
shipboard velocity data, hydrographic profiles as well as oxygen and nutrient concentration measurements from the
135   ~~repeat~~repeated measurements ~~at~~along 12° S.

2.1.1 Shipboard velocity observations

~~During the cruises upper~~Upper ocean velocities were recorded continuously using two vessel-mounted Ocean Surveyor
Acoustic Doppler Current Profiler systems (vmADCP) installed on R/V Meteor. One vmADCP was ~~operating~~operated at a
frequency of 75 kHz (OS75~~). System~~) and its system configuration during the cruises varied only in depth bin settings. Depth
140   bins of 4, 8 or 16 m were chosen depending on strength of the backscatter signal and the focus of the investigation~~.~~, allowing
a maximum range of 750 m. The second vmADCP operated at 38 kHz (OS38) ~~which~~and recorded depth bins of ~~32m~~32 m
while sampling an ~~increase~~increased depth range (30~~ 1000m) compared to the OS75 system.~~ – 1000 m). During post-
processing, vmADCP velocities were corrected using a mean amplitude and misalignment angle determined from water-track
calibration (e.g. Fischer et al., 2003). Misalignment angles derived from individual ship accelerations and turns followed a
145   Gaussian distribution having a standard deviation of less than 0.65° for the OS75 and less than 0.75° for the OS38 (Sommer
et al., 2019). A temporal trend was not detectable. The uncertainty of the misalignment angle calibration can be determined
from its standard deviation divided by the square root of the number of independent estimates (e.g. Fischer et al., 2003). For
our data, more than 100 independent estimates were available for each cruise, resulting in an angle uncertainty of less than
0.1° and an associated velocity bias of less than 1 cm s^{-1} for underway data. Fischer et al. (2003) suggested an accuracy of 3
150   cm s^{-1} for hourly underway data recorded during calm conditions in the tropics.

2.1.2 Hydrographic observations

~~At~~Along the 12° S section~~,~~ a total of 151 hydrographic profiles were collected during ~~the~~ cruises M136 and M137 with a
lowered SeaBird SBE 9-plus conductivity-temperature-depth (CTD) system using ~~two pumped oxygen,~~double sensor packages
for temperature~~ and,~~ conductivity ~~sensors each~~and oxygen. The CTD was attached to a General Oceanics rosette with 24 Niskin
155   bottles of 10 l to collect water samples. For the calibration of the conductivity sensor~~,~~ water samples were analysed with a
Guildline Autosal Salinometer model 8400 B. Correction coefficients for the CTD's conductivity sensors were derived using

4

a multiparameter fit of the Autosal conductivities against the uncalibrated CTD sensor measurements. ~~Coefficients included an offset and factors for temperature, pressure and conductivity.~~

CTD oxygen sensors were calibrated against oxygen concentrations determined from bottle water samples using Winkler titration (Winkler, 1888; Grasshoff et al., 1983). Processing and calibration followed the GO-SHIP recommendations (Hood et al., 2010). Previous studies using Switchable Trace amount OXygen (STOX) sensors have shown that the core of the Peruvian OMZ is functionally anoxic (Revsbech et al., 2009; Thomsen et al., 2016). Unfortunately, the Winkler titration method fails to accurately determine very low oxygen concentrations from bottle water samples. To assure anoxic conditions in the OMZ core, a mean oxygen concentration offset of 2.26 µmol l^{-1} was subtracted from low oxygen values. Calibration of the salinity and oxygen sensors was performed separately for each cruise, except for M136 where the mean of the calibration of the preceding and succeeding cruises M135 and M137 was used (M136 lacked ~~the required~~ deep-water samples required for calibration purposes). The final post-cruise calibration of the data resulted in an accuracy for temperature, salinity, and oxygen of 0.002° C, 0.002 g kg^{-1} and 1.5 µmol kg^{-1}, respectively.

2.1.3 Nutrient measurements

Water samples collected during the upcast of the CTD rosette were used to determine nutrient concentrations. Concentrations of nitrate, nitrite and phosphate were measured using a QuAAtro autoanalyzer (Seal Analytical) with ~~the~~a precision of 0.1 µmol l^{-1}, 0.1 µmol l^{-1}, and 0.2 µmol l^{-1}, respectively (Sommer et al., 2019). Ammonium concentrations were measured using a fluorimetric method (Holmes et al., 1999).

In addition, concentrations of nitrate were measured using a Satlantic Deep Submersible Ultraviolet Nitrate Analyzer (SUNA) mounted on the CTD rosette~~.~~ (Hauschildt et al., 2020). SUNA measurements are based on the absorbance spectra of ultraviolet light (Sakamoto et al., 2009). Data post-processing followed Karstensen et al. (2017) and Thomsen et al. (2019). In a final step, the SUNA nitrate concentrations were calibrated against the nitrate concentrations from the CTD water samples using a linear fit.

2.2 Additional data

~~To~~Additional regional data sets from satellite observations were used to supplement our analysis of ship-board observations ~~we used additional data sets.~~. Sea Level Anomaly (SLA) data based on satellite altimeter measurements were ~~used~~ provided by the E.U. Copernicus Marine Environmental Monitoring Service (product: SEALEVEL_GLO_PHY_L4_REP_OBSERVATIONS_008_047). This is a level 4 dataset derived by merging all available satellite altimetry data into one gridded product. Reprocessed data from January 1, 1993 to January 1, 2018 with the release days January 15, 2018 (data before May 15, 2017) and May 16, 2018 was accessed. Additionally, sea surface temperature from the NOAA Extended Reconstructed Sea Surface Temperature, Version 5 (ERSSTv5) dataset (Huang et al., 2017a) was analyzed. This dataset provides monthly values of SST on a 2°x2° grid based on in-situ temperature observations from several sources (Huang et al., 2017b). Finally, ~~we analysed~~ wind stress data from the ASCAT product of satellite scatterometer winds (Bentamy and Fillon, 2012~~).~~) was analyzed. This product provides daily global winds and wind stress data with a resolution of 0.25°.

3 Methods

3.1 Analysis of velocity observations

The continuous velocity recording was split into segments when the ship was moving in on- or offshore directions only. The velocities were rotated to derive the alongshore component and then a mean velocity section was calculated for each segment of the cruise in 2 km bins according to offshore distance. Periods where the ship was moving slower than 1 kn were excluded.

To derive the sections of alongshore velocity over longer time periods, the data from several of these segments were averaged. The presented sections were smoothed using a ~~2D~~2-D Gaussian ~~weighting with an influence radius of 4 km (8 m) and a cut-off of 6 km (18 m) horizontally (vertically).~~weights.

3.2 Analysis of hydrographic and biogeochemical data

200 The analysis of hydrographic data ~~is~~was based on the TEOS10 definitions (IOC et al., 2010~~) and conservative~~). Conservative temperature, absolute salinity, density and ~~(~~potential~~)~~ density anomalies were calculated with the Matlab Gibbs Seawater Toolbox (McDougall and Barker, 2011; Version 3.05). Nutrient concentrations were transformed to µmol kg^{-1} to remove the effect of compressibility on vertical gradients. In the following we mean conservative temperature when we refer to temperature and absolute salinity when we refer to salinity.

205

3.2.1 Nitrogen deficit

In suboxic environments, microbially mediated ~~biogeochemical~~ processes such as denitrification and anaerobic ammonium oxidation (anammox) transform biologically available reactive nitrogen ~~nutrients~~ (nitrate, ~~nitrate~~nitrite, and ammonium) via intermediate steps into ~~a form unusable~~ dinitrogen (N_2), which cannot be used by most organisms~~.~~ (dinitrogen, N_2). These

210 processes lead to a loss of reactive nitrogen ~~nutrients (N loss)~~ relative to other nutrients such as ~~phosphorus. A metric for N-loss processes is the nitrogen deficit. A deficit (or excess) in nitrogen exists when the ratio~~phosphate (PO_4^{3-}). The global distribution of ~~nitrogen to phosphorus deviates from the ratio associated~~nitrate, phosphate and dissolved inorganic carbon (DIC) display a strong covariation, with ~~the synthesis and remineralisation~~a slope of N:P of about 16:1 reflecting the mean stoichiometry of organic matter~~, i.e. the Redfield ratio~~ synthesis and degradation. In order to analyze the impact of nitrogen

215 loss and N_2-fixation on the NO_3^- distribution it is convenient to remove the photosynthesis/remineralization trend and only focus on deviations, N*, from this trend. The concept of N* has been introduced (Gruber ~~and~~& Sarmiento~~,~~ 1997, 2002). Here, ~~we used~~ the formulation of Chang et al. (2010) was applied to investigate the nitrogen deficit, N_{def}, µmol kg^{-1}. It is based on the deviation from the ratio between nitrogen species and phosphate outside of the eastern tropical south Pacific OMZ. The nitrogen deficit is calculated as:

220 $$~~N_{def}~~N_{def} = 15.8\ (PO_4^{3-} - 0.3) - (NO_3^- + NO_2^- + NH_4^+) (1)$$

Where PO_4^{3-}, NO_3^-, NO_2^-, and NH_4^+ are the concentrations of phosphate, nitrate, nitrite and ammonium, respectively. With this definition, positive values of N_{def} quantify ~~the~~an N-loss that has occurred within a certain water mass while it ~~has~~ remained ~~within~~in the Peruvian OMZ.

225 ### 3.2.2 Section averaging

~~Hydrographic~~Smoothed hydrographic and biogeochemical properties along the 12° S section ~~analysed in this study~~ were calculated by ~~first~~ interpolating the data vertically onto common potential density surfaces. ~~Performing subsequent analysis~~Averaging in density space removes the effect of ~~internal waves which cause elevated variability of~~ signal smearing due to vertical displacement ~~of properties in the water column.~~caused by internal waves. The profiles were then averaged in

230 bins of 2 km according to distance from the coastline~~. The data were~~ and then smoothed using ~~a 2D~~2-D Gaussian ~~weighting with a density influence range (standard deviation of the Gaussian distribution) of 0.03 kg m^{-3} and a cut off range of 0.05 kg m^{-3} and respectively an influence and cut off range of 3 and 6 km within 40 km of the coast, 7 and 15 km for the distances between 40 km and 80 km offshore and 15 and 20 km for more than 80 km offshore. The decreasing scale of horizontal interpolation towards the coast was used to benefit from the increased number of profiles to preserve smaller scale features.~~

235 ~~Finally~~weights. In a final step, the averaged and ~~interpolated properties~~smoothed sections were vertically transformed back into depth space using the smoothed depth – density relation.

3.3 Sea level anomaly and wind data

The local SLA along the 12° S section was calculated by first averaging all daily gridded SLA data between 12° and 12.5° S over the time periods used for the velocity sections and interpolating them onto the section according to the distance to the

240 coast. Grid points closer than 30 km to the coast ~~have been~~were excluded. ~~The~~Then the mean SLA along the section was subtracted to focus on the cross-shore gradient. ~~Intraseasonal~~In addition, intraseasonal variability along the equator and coastline was analysed by subtracting the mean SLA over the 25-year time series before bandpass filtering SLA using a 4th order Butterworth filter for a time window between 20 and 90 days. To follow intraseasonal SLA variability due to propagating waves along the equator and subsequently along the western South American coast, we used bandpass filtered SLA data

245 averaged between 0.25° S and 0.25° N from the equator and two-grid-points averages from near the coast.

For investigating wind forcing of Kelvin waves at the equator, SLA and zonal wind anomaly were averaged to five-day means over 10° of longitude. Additionally, wind anomaly was averaged between 5° N and 5° S while SLA was averaged between 2° N and 2° S.

3.4 Theoretical coastal trapped wave structure

250 To interpret the observed flow variability along the Peruvian coast in terms of CTWs, the cross-shore-depth structure of CTWs was determined by considering the linear, hydrostatic, inviscid, and Boussinesq approximated equations of motion on an f-plane using local bathymetry and stratification (Brink, 1982; 1989; Illig et al., 2018a). For alongshore scales larger than cross-shore scales and horizontally uniform stratification, cross-shore-vertical mode structures (eigenfunctions) and corresponding phase velocities (eigenvalues) solutions ~~can be~~were obtained from the simplified set of equations by using a resonance iteration

255 approach (Brink, 1982; Brink and Chapman, 1987). Here, we obtained the eigenfunctions and eigenvalues for the first three modes by applying a modified version of the Brink and Chapman (1987) Coastal-Trapped Wave programs as published by Brink (2018). ~~These solutions have been used successfully in previous analyses of CTW structures in observational and model data (e.g. Brink et al., 1982; Pietri et al., 2014; Illig et al., 2018a).~~

Local bathymetry and stratification are required as input to Brink's (2018) set of Matlab mfiles. The cross-shore distribution

260 of bathymetry was taken from the multi-beam echo sounder data collected during the cruises along 12° S. Echo sounder data was averaged in 5 km bins which resulted in a monotonic increase of water depth in an offshore direction. ~~Water~~The maximum water depth ~~lower than~~used for the wave solutions was 5000 m ~~were ignored.~~. From two offshore CTD profiles (M136 #60 and M137 #92) exceeding 3000 m depth, a stratification profile was calculated first for each profile using 20 data points with 1 dbar spacing and then a mean profile was calculated from both casts in 5 m intervals.

265 **4 Results**

4.1 Variability of the boundary circulation

~~Direct~~The direct velocity observations from the multi-cruise program ~~allow~~allowed a detailed ~~description~~assessment of the variability of the eastern boundary alongshore velocity structure at 12° S for a period of more than eleven weeks (Fig. 2). During the observational period from early April to June 24~~,~~ (2017~~,~~), we captured an event of strongly increased poleward

270 flow that started in early May and lasted for about 35 days.

The time series started with two days of sampling in April 7 to 8. During this period, a distinct poleward flowing PCUC was present that extended 80 km offshore (Fig. 2a) and had maximum velocities of more than 0.3 m s^{-1} on the continental shelf. Satellite altimetry indicated an increasing SLA towards the coast (Fig, 2a upper subpanel). Between April 18 and May 26, and

except for a short break from May 4 to 6, the 12° S section was continuously ~~occupied~~surveyed. In mid-April, a poleward flow was present only on the shelf (Fig. 2b). However, from the end of April to mid-May, the PCUC considerably strengthened reaching maximum core velocities of about 0.5 m s^{-1} between 50 and 100 m depth 50 km offshore (Fig. 2c, d and e). Furthermore, ~~its~~the PCUC poleward flow extended to more than 80 km offshore and ~~it~~occupied the ~~whole~~ water column above 400 m depth. The SLA increased towards the coast (by 2 cm over 40 km) implying that a poleward geostrophic velocity anomaly was present at the sea surface as well. Towards the end of May, poleward flow in the PCUC did not increase further, but remained at a similar level as during mid-May (Fig 2f). In ~~contrary~~contrast, velocity data from a final section occupation 3 weeks later in June 24 shows evidence that the PCUC had weakened drastically (Fig. 2g), exhibiting a comparable velocity distribution as ~~between~~for the period April 18-25 (Fig. 2b). Assuming similar time scales for its deceleration as for ~~it~~its acceleration, the period of intensified PCUC flow was between 30 to 40 days. The intensified PCUC flow strongly ~~exceeds~~exceeded the climatological PCUC flow reported from this region. Mean alongshore flow at 12° S determined from vmADCP data sampled during 22 cruises ~~show~~showed maximum PCUC core velocities of 0.1 – 0.15 m s^{-1} (Chaigneau et al., 2013), similar to the situation observed during April 18-25 and June 24 (Fig. 2b and g).

In April, the velocity sections indicated an equatorward flow offshore and below the PCUC (Fig. 2). ~~At these depth and offshore ranges, the~~The Peru Coastal Current and the Chile-Peru Deep Coastal Current are thought to be located at these depths and offshore ranges (e.g. Penven et al., 2005; Chaigneau et al., 2013). In late April, the equatorward flow increased in strength and extended to shallower ~~depth~~depths (Fig. 2b and c). However, during the period of strong poleward flow in May, the equatorward flow decreased and was present only below 400 m depth close to the offshore end of the section (Fig. 2e and f). On June 24, a weak equatorward flow was present below 200 m at most parts of the section but never reached velocities of 0.1 m s^{-1}. We found no indication of equatorward flow above or inshore of the PCUC, where the equatorward surface jet is expected to be situated. The lack of this surface flow in observations was also ~~previously~~ noted by Chaigneau et al. (2013).

To compare the alongshore circulation with hydrographic and biogeochemical sampling, the data were averaged into two periods: The initial phase of weak poleward flow (Fig. 3a) covering the period from April 18 – May 3, and a period of enhanced poleward flow 12 – 26 May (Fig. 3b). The increase ~~of~~in poleward velocities ~~is~~was especially strong between 40 and 60 km offshore where velocities ~~increase~~increased from about zero to 0.4 m s^{-1} (Fig. 3c). The core of velocity increase ~~is extending~~extended deeper than the intensified PCUC and ~~is~~was more detached from the coast.

4.2 Potential causes of circulation variability

4.2.1 Role of local wind stress

~~A~~Changes in the local wind stress curl are a potential local forcing mechanism of ~~the~~an intensified PCUC flow ~~are anomalies of local wind stress curl.~~. An increase in the magnitude of near-coastal negative wind stress curl leads to an increased poleward flow along the eastern boundary through Sverdrup dynamics (e.g., Marchesiello et al., 2003). The adjustment of the circulation to changes in the wind stress curl at the eastern boundary is rather fast and occurs within a few days (Klenz et al., 2018). Wind stress curl along the Peruvian continental margin between 10° S and 14° S was negative throughout the observational period (Fig. 4), continuously forcing poleward flow. However, during the period of PCUC acceleration between end of April and mid-May, the magnitude of negative wind stress curl decreased (Fig. 4c, d, e, f). It can thus be ruled out that local wind stress curl forcing is responsible for the observed intensified PCUC. Nevertheless, elevated negative wind stress curl was observed from May 18 – 22, which may have contributed to ~~maintaining~~maintain a strong PCUC in late-May.

Variability of near-coastal alongshore wind stress excites CTWs ~~which~~that propagate poleward (e.g. Yoon and Philander, 1982) and thereby ~~enhance~~enhances or ~~decrease~~decreases poleward flow within the depth range of the PCUC. ~~Model studies show that CTWs are excited near the equatorward edge of the region of wind variability (e.g. Fennel et al., 2012). In Mid-April through~~From mid-April until May 2017, alongshore wind stress between 6° S and 15° S was variable (Fig. 5). While moderate wind stress (0.03 – 0.06 N m^{-2}) prevailed from mid-April to May 3, it was weak during the first two weeks of May

(Fig. 5d, e, g). ~~However, during the later period the strong acceleration of the poleward flow occurred, requiring an intensification of alongshore wind stress. Thus, the initial acceleration of the PCUC during this period (Fig. 2d, e) cannot be related to local wind stress variability. Alongshore wind stress did significantly strengthen on~~On May 15~~-~~, the wind stress increased and remained elevated for a period of about 5 days. This wind ~~event was intense between 15° and 8° S, but did not~~

320 ~~occur north of 8° S. CTWs were likely excited in the region between 12° and 8° S that contributed to the elevated poleward velocities~~ variability cannot explain the observed ~~in the later phase between May 17 and 26 (Fig. 2f).~~changes in poleward transport. The poleward transport increased from late April to its maximum mid-May, whereas the alongshore wind stress during this period decreased in the first week and then increased seven days later.

4.2.2 Equatorial winds and wave response~~.~~

325 ~~A~~According to equatorial linear wave theory a weakening of the trade winds at the equator by e.g. westerly wind events ~~forces downwelling on the equator,~~ generates ~~an~~eastward propagating equatorial Kelvin ~~waves, which in turn may have transmitted~~ wave. Once the equatorial Kelvin wave interacts with the eastern boundary parts of its energy are transmitted to a CTW ~~at the eastern boundary.~~(Enfield et al., 1987). Indeed, several westerly wind anomalies occurred in the central and eastern equatorial Pacific during the first 6 ~~month~~months of 2017 (Fig. 6). A particularly elevated westerly wind anomaly occurred between the

330 international date line and 120° W ~~occurred~~ during the first two weeks of April (Fig. ~~7a). A~~6a). In response, a positive SLA propagating along the equator ~~appears~~appeared to the east of the wind event ~~at~~between about 100° W ~~(Fig. 7b).~~
~~This behaviour is similar to the appearance of the positive signals in the filtered SLA only east of 95°~~and 80° W (Fig. ~~6). A negative SLA anomaly occurs in the western equatorial Pacific at the time of the wave propagation and earlier (Fig. 7b) which may have been forced by the easterly wind anomaly at 160° E (Fig. 7a). But the SLA (Fig. 7b) reveals that the propagating~~

335 ~~negative SLA seen in filtered data (Fig. 6) does not occur throughout the basin and in the eastern Pacific the local minimum between phases of higher SLA is exaggerated by the filter. A downwelling CTW causes an increase of the PCUC, an increase of SLA and downward movement of subsurface isopycnal. The SLA and PCUC change suggest the existence of a wave of this sign. A first mode downwelling CTW would induce poleward transport across the upper 1500 m and we see poleward transport throughout the measurement range in the upper 1000 m. The existence of positive of a coherent high SLA along the~~

340 ~~eastern Equator and the South American coast with poleward propagation does support the existence of a downwelling wave generated around 95° W as well, while the speed of the propagation suggests a first mode wave.~~

~~Similar to the velocity structure, SLA signals also support an association of the intensified poleward flow to the passage of a downwelling CTW. A downwelling CTW is associated with an upward elevation of the sea surface and a compensating~~

345 ~~downward displacement of the isopycnals in the water column as well as an intensification of poleward flow (e.g.~~ 6b dash line, Fig. 7) and arrived at the eastern boundary at the beginning of May.~~Echevin et al., 2014). In this study we use the designation "downwelling" only to indicate the sign of velocity and SLA anomalies associated with the CTW. As discussed in the previous section, a local SLA increase was observed at the Peruvian coast while elevated poleward velocities within the PCUC depth range were present.~~

350 Bandpass-filtered SLA data from the equator and from near the continental slope (section 3.3) ~~indicates a positive SLA off Peru and Ecuador between the equator and about 14° S during this period (Fig. 6). The positive SLA along the coast propagates poleward at a velocity not inconsistent with a propagation speed of 3.1 ms⁻¹, the phase speed of the first CTW mode (Fig. 5). Moreover, when looking at SLA along the equator, there is a coherent signal starting at about 95° W moving towards the~~along the South American continent (Fig. 7) indicate that the positive SLA arriving at the eastern boundary continued southward

355 along the eastern boundary ~~and arriving at~~to about 14° S. Along the ~~same time when~~equator, the ~~SLA maximum of the coast is developing. Again, signal~~propagation ~~from west to east is indicated,~~speed of the SLA was about 2.7 m s⁻¹ (dashed line in the left panel of Fig. 7), which agrees with the ~~phased~~phase speed of a first vertical mode equatorial Kelvin waves (e.g. Yu

9

and McPhaden, 1999). ~~The SLA indicates the propagation of negative anomalies corresponding to an upwelling wave about 20 days earlier and with origin west of 140° W (Fig. 6) the arrival of this potential upwelling wave fits with the downward tilt in the SLA between April 25 and May 3 (Fig. 2c) and may contribute to the weak poleward flow by causing equatorward velocity anomalies.~~The speed of propagation of the SLA signal along the eastern boundary was somewhat enhanced and around 3 m s^{-1}. A positive SLA signal was associated with a negative (downward) displacement of the thermocline, eastward upper-ocean velocities at the equator and poleward upper-ocean velocities at the continental slope. This agrees well with the SLA signal and the increased poleward PCUC velocities at 12° S and suggests the existence of a downwelling CTW during May 2017. Additionally, the speed of propagation at the equator indicates a first baroclinic mode Kelvin wave arriving at the eastern boundary.

4.~~1~~2.3 Modal structure of the intensified flow

~~The~~To further investigate the nature of the boundary flow intensification, the cross-shore-depth structure of alongshore velocity ~~obtained~~was determined for the first three CTW modes at ~~the~~ 12° S ~~section (~~(Fig. 8, see section 3.4~~) varies~~ for a description of the model used). Due to a steep continental slope at 12° S, the velocity structure of the different CTW solutions varied predominately in the vertical axis with poles of opposing velocity located above each other (Fig. ~~7~~8). Flow reversal for each individual mode away from the boundary occurs at shallower depth ~~away from the boundary~~ compared to inshore regions. ~~As expected, higher~~Higher modes exhibit an upper pole of enhanced velocity located at shallower depth compared to lower modes ~~and the phase speed (Fig. 7) decreases. The obtained phase speeds are within ranges reported by Illig et al. (2018a, their table 1) for the first two modes while the phase speed of the third mode is slightly lower (0.82 ms^{-1} compared to 0.93±0.08 ms^{-1}). The velocity structure of the modes is very similar to their structure reported in their study at 16° S as well.~~.

For comparison, ~~we show~~Fig. 8e shows the difference of full-depth ~~OS38~~low-frequency vmADCP alongshore velocities between May 12 ~~–~~to 26 and April 18 ~~–~~to May 3 ~~(Fig. 7e).~~. Apart from the increased poleward velocity in the upper 500 m, the alongshore velocity difference ~~is~~resolved by the OS38 was weakly poleward throughout the upper 1000 m of the water column ~~resolved by the OS38~~ (Fig. ~~7e). When comparing~~8e). Comparing the baroclinic structure of the observations to the baroclinic structure of the different CTW modes, ~~it becomes obvious that due to~~ the missing flow reversal~~,~~ in the upper 1000 m shows that the observed change in alongshore velocity is best described by a first mode CTW. This mode features poleward flow anomalies throughout the upper 1500 m (Fig. ~~7b~~8b) which agrees with the distribution of the velocity differences between the two time periods throughout most of the upper 1000 m (Fig. ~~7e~~8e). The maximum increase of poleward flow, on the other hand, ~~is~~was restricted to a depth range similar to the upper poleward velocity core of a second mode CTW.

Additional support for the presence of first mode CTW originates from a comparison of the phase speeds. At 12° S, the local phase speeds of the model CTW modes (Fig. 8) were higher than those for equatorial Kelvin waves. In particular, the phase speed of the first mode CTW was 3.1 ms^{-1}, which agrees very well with the phase propagation of the SLA signal discussed in section 4.2.2.

4.3 Response of hydrographic conditions to the PCUC intensification

In the following~~,~~ we analyse the changes in hydrographic conditions co-occurring with the increase of the alongshore flow. Lower near-surface ~~conservative~~ temperatures near the coast compared to offshore (Fig. 1, Fig. ~~8a~~9a, b) indicated active upwelling during the observational program. While the upwelling signal was restricted to the upper 50 m, near-coastal water masses between 50 m and 300 m were significantly warmer compared to water masses offshore (Fig. ~~8a~~9a). During the intensified PCUC period (Fig. ~~8~~9 middle panels~~)~~). the cross-shore temperature gradient intensified, leading to an increased downward displacement of isopycnals and isotherms near the coast (Fig. ~~8b~~9b). There, the associated warming signal between ~~100m~~100 m and 200 m depth was up to 0.5° C. ~~It note~~Note that during the PCUC intensified period, near-coastal surface temperatures decreased.

~~Absolute salinity~~Salinity featured a shallow subsurface salinity maximum at about 25 m depth originating offshore and extending over the slope and shelf (Fig. ~~8d~~9d and e). As for temperature, cross-shore salinity gradients were evident between 50 and ~~300m~~300 m depth with higher salinities near the coast which intensified when the PCUC increased. At the same time, salinity at the upper shelf decreased (Fig. ~~8f~~9f).

Distribution of oxygen concentrations were characterized by a sharp oxycline above the anoxic OMZ (Fig. ~~8g~~9g and h). During the weak PCUC period, oxygen concentrations decreased from slightly supersaturated ~~concentrations~~ at the surface to anoxia within the upper 100 m of the water column (Fig. ~~8g). At depth between~~9g). Between 450 and 500 m, oxygen concentrations started to increase again to detectable values (Fig. ~~8g~~9g). When the poleward flow intensified, oxygen levels of waters below about 100 m depth increased (Fig. 9i) and low oxygen waters were found deeper in the water column ~~following~~than previously (Fig. 9h). Part of the increased oxygen levels were due to the downward displacement of the isopycnals (Fig. ~~8h). During this period~~9h), particularly in the near-bottom waters above the continental slope. There, oxygen concentrations ~~of~~larger than 2 µmol kg⁻¹ were ~~found~~observed at 200 m depth in ~~the bottom~~ bottom waters (Fig. 9h), a depth range that is usually occupied by anoxic water ~~(Fig. 8h), which has~~masses. Such ventilation events have significant consequences for benthic and pelagic biota and for biogeochemical processes in that depth range, as further discussed below.

In the upper water column above 400m, waters ~~denser~~with potential density anomalies larger than ~~102525~~.9 kg m⁻³ were ~~mainly~~predominantly Equatorial Subsurface Water (ESSW; Fig. ~~9~~10). ESSW originates from the equatorial current system. It is characterized by a linear relationship of temperature and salinity in the temperature range 8 – 14 °C and ~~absolute~~ salinity range 34.6 – 35.0 (e.g. Grados et al., 2018). Lower salinity Eastern South Pacific Intermediate Water (temperature range 12 – 14 °C, salinity 34.8), which is also situated in the depth range mentioned above, was only observed in the hydrographic data from two offshore stations (Fig. ~~9a~~10a). The dominance of ESSW was not affected by the increasing poleward velocities (Fig. ~~9b~~10b) and most profiles ~~follow~~followed the same temperature and salinity relationship in both phases. In fact, during PCUC intensification, the ESSW was the sole water mass in the upper ~~400m~~400 m within 80 km of the coast (Fig. ~~9b~~10b).

4.4 Response of nutrient biogeochemistry to ~~the~~ PCUC intensification

~~Nutrients are transported poleward by the PCUC and their advection thus is likely influenced by the variability of poleward velocity. In the following we describe the observed changes in nutrient concentrations and relate them to the variability in PCUC strength.~~

~~Nitrate~~Nutrients are supplied to the upwelling region by poleward transport within the PCUC. In the following, we relate the observed changes in nutrient concentrations to the PCUC variability and to microbially-mediated biogeochemical processes (section 3.2.1). In the anoxic core of the OMZ denitrification represents a prominent process of anaerobic organic matter degradation and a major sink for reactive nitrogen (Kavelage et al., 2013, Gruber 2008). During denitrification, nitrate is stepwise reduced to N₂, with nitrite and nitrous oxide, as important intermediate products. Subsequently, nitrite is either further reduced to N₂ via denitrification or may be used in the microbially driven anaerobic oxidation of NH₄⁺ to N₂ known as annamox (Kuypers et al. 2005, Lam et al. 2009), which leads to a loss of reactive nitrogen. The distributions of nitrate (Fig. 11a and b) and nitrite concentrations (Fig. 11d and e) demonstrate the transformation of nitrate to nitrite. In the open ocean nitrate increases with depth in the upper 1000 m, whereas on the Peruvian margin a nitrate minimum in the anoxic core of the OMZ is pronounced at 12° S (Fig. 11a and b), co-occurring with a maximum in nitrite.

During the period of PCUC intensification, nitrate concentrations on the shelf and upper slope increased ~~when the poleward flow strengthened (Fig. 10a and b). The nitrate concentrations were low at the surface and increase with depth (Fig. 10a and b). During the initial phase, offshore surface~~(Fig. 11a and b). Before the intensification, nitrate concentrations ~~decreased to less than 10 µmol kg⁻¹ and increased below to 20 µmol kg⁻¹ at 50 m and 25 µmol kg⁻¹ at~~ in the upper 300 m ~~depth (Fig. 10a). Low~~of the water column hardly exceeded 25 µmol kg⁻¹ and particularly low concentrations were found in bottom waters on the shelf ~~were most prominent between 75 and 100 m depth going down to~~, where a local minimum with less than 15

11

µmol kg⁻¹ is reached ~~(Fig. 10a). After the intensification of~~(Fig. 11a). As the PCUC intensified, nitrate concentrations between 50 ~~and 100~~ m ~~depth offshore~~ and 250 m ~~in bottom waters increased and exceed~~mostly exceeded 25 µmol kg⁻¹ (Fig. ~~10b~~11b). Throughout this part of the section, the increase ~~exceeded~~was higher than 2.5 µmol kg⁻¹ (Fig. ~~10c), including~~11c), and in some ~~areas with an increase in excess of 5 µmol kg⁻¹ and even up to 10 µmol kg⁻¹. The surface layer featured an~~increase in ~~excess of 5 µmol kg⁻¹ as well (Fig. 10c).~~exceeded 5 µmol kg⁻¹.

~~Nitrite~~On the other hand, nitrite concentrations in ~~the~~deeper and bottom ~~water~~waters on the shelf and upper slope were reduced ~~by~~during the intensified PCUC period (Fig. ~~10d~~11d and e). ~~The~~In general, nitrite concentrations ~~were low outside of the OMZ and their structure~~in oxygenated waters (O₂ > 2 µmol kg⁻¹) were less than 1 µmol kg⁻¹, which is likely due to nitrification. In the anoxic core of the OMZ, the nitrite distribution featured two maxima~~, the main;~~ one ~~located~~in the upper part of the OMZ between 150 m and 200 m depth and another in the centre of the OMZ ~~around~~at 300 m depth ~~and the secondary maximum in the upper part~~, both having concentrations of ~~the OMZ at 150~~up to ~~200 m depth. After~~5 µmol kg⁻¹. During the PCUC intensification ~~of the PCUC~~period, the upper boundary of nitrite containing water was displaced downwards~~, leaving bottom waters above 250 m depth free of nitrite~~ (Fig. ~~10e). The depletion of nitrite in the bottom water was coupled to a weak ventilation supplying oxygen~~11e) following the displacement of anoxic waters (Fig. ~~8h).~~9h). This caused a nitrite decrease exceeding 2 µmol kg⁻¹ in the deeper and bottom water ~~around~~on the continental slope at about 200 m depth (Fig. ~~10f~~11f). Ammonium concentrations were generally low or undetectable. Concentrations in excess of 0.4 µmol kg⁻¹ occurred only ~~on the upper shelf and~~ close to the surface on the upper shelf (Fig. ~~10g~~11g and h~~), and were indicative of remineralisation of phytoplankton detritus, with rapid removal over time of~~). It should be noted that in the Peruvian upwelling region, the sediments are a strong source of ammonium ~~due to phytoplankton uptake and nitrification. The patchiness of~~(e.g. Sommer et al., 2016). However, despite taking water samples for nutrient analysis very close to the sea floor, elevated ammonium concentrations ~~caused high positive and negative differences very close to each other on the shelf (Fig. 10i). In the surface layer above 50 to 80 m in offshore waters, a decline~~could not be detected, suggesting a fast removal by annamox of ammonium ~~concentrations~~which was ~~observed~~released from the sediments. In case oxygen was present, ammonium could also have been nitrified to nitrate.

Phosphate concentrations did not change ~~strongly by the increased strength of~~considerably during the PCUC intensification period (Fig. ~~10j~~11j and k). Concentrations were low at the surface and increased to 2 µmol kg⁻¹ at 50 m depth. Within the upper OMZ, the concentrations were higher offshore than onshore (Fig. ~~10j~~11j and k). When the PCUC intensified, concentrations decreased ~~below 50 m depth and above 100 m at 80 km offshore and 300 m inshore (Fig. 10l).~~in approximately the same region in which the nitrate increase occurred (Fig. 11l). A phosphate decrease of up to 0.3 µmol kg⁻¹ occurred in bottom waters on the shelf at water depths shallower than 100 m.

The nitrogen deficit (N_{def}, section 3.2.1) was reduced ~~in~~during the ~~later phase~~period of ~~the strong~~ PCUC intensification (Fig. ~~10m and~~11m, n~~). During~~ and o). Whilst the ~~weak~~ PCUC ~~phase the offshore maximum deficit~~ was ~~located between 150 and 200 m depth exceeding 12.5 µmol kg⁻¹ and the absolute maximum was a localized peak exceeding 15 µmol kg⁻¹ in bottom~~weak, waters ~~just above 100 m depth (Fig. 10m). This maximum on the shelf was caused by low nitrate (Fig. 10a and high phosphate concentrations (Fig. 10j), while nitrite (Fig. 10d) and ammonium (Fig. 10g were enhanced as well. After the PCUC intensification the deficit reached 5 µmol kg⁻¹ at about 70 m depth offshore and 200 m depth at the coast (Fig. 10n). At greater depths the maximum deficit exceeding 12.5 µmol kg⁻¹ was located offshore around 150 m depth, extending towards the coast along isopycnal surfaces. After the PCUC intensification, the~~having a nitrogen deficit ~~in~~between 5 µmol kg⁻¹ and 15 µmol kg⁻¹ were present at depths between 100 m and 400 m. Maximum values were found on the continental shelf and offshore between 100 m and 200 m (Fig. 11m). During the PCUC intensification period, the nitrogen deficit maximum at the continental shelf disappeared and low deficit waters (N_{def} < 5 µmol kg⁻¹) occupied the upper 200 m of the water column inshore of ~~70~~40 km ~~was reduced~~ (Fig. ~~10o~~11n). The ~~maximum decrease of the deficit occurred in the bottom water just above 100 m depth~~

12

exceeding 10 µmol kg⁻¹; here the maximum described above in Figure 7(m) disappeared with the PCUC intensification. Further offshore around 100 m depth the decrease of the deficits exceeded 5 µmol kg⁻¹ in several patches as well (Fig. 10o).

485 ~~The decrease in nitrogen deficit between 50 m depth and about 200 m depth (deeper toward the coast, and shallow offshore) exceeding 5 µmol kg⁻¹ in its maximum agreed~~reduced nitrogen deficit was due increased nitrate concentrations (Fig. 11c) and somewhat reduced phosphate concentrations (Fig. 11l). Furthermore, the region with reduced N_{def} agrees well with the location of ~~largest~~maximum poleward flow ~~(Fig. 3b). At this vertical and horizontal range nitrate was increasing by more than 2.5 µmol kg⁻¹ (Fig. 10c) and phosphate decreased (Fig. 10l), both changes contributed to the reduced nitrogen deficit. Nitrite~~

490 ~~concentrations decreased as well (Fig. 10f), but the total increase in nitrogen species still exceeded the phosphate decrease by more than the ratio implied in equation (1), with the nitrate change, dominating the change of nitrogen species.~~

~~The increase in nitrate concentrations and the decrease of the nitrogen deficit and phosphate concentrations are strongest in the upper 200 m where the intensified PCUC had its maximum during the same time period. These changes occurred when comparing both regimes in density space as well (not shown) and a nitrate increase within the ESSW was evident~~during the

495 PCUC intensification period (Fig. 3b). This suggests that poleward advection in the intensified PCUC ~~is~~was the main cause for the observed changes in biogeochemical properties ~~while changes due to vertical displacement only play a minor role, here.~~.

5 Summary and Discussion

500 Measurements from an intensive physical and biogeochemical shipboard sampling program off Peru at 12° S carried out between April 7 and June 24 2017 are used to analyse intraseasonal variability of the eastern boundary circulation and associated changes in hydrography and nutrient distributions. The Our most prominent finding is an intensification of poleward ~~velocities~~flow within the depth range occupied by the PCUC that ~~occurred throughout the last 3 weeks of~~started early May ~~in~~
2017~~.~~ and lasted for about 35 days. During this period, ~~maximum~~ poleward velocities occupied the whole water column above

505 1000 m depth and extended to more than 80 km offshore. Maximum velocities in the PCUC core between 50 m and 100 m depth were above 0.5 m s⁻¹ ~~exceeding~~, about 5 times larger than the ~~reported mean state by far (e.g.~~respective climatological PCUC velocities (Chaigneau et al., 2013~~). The poleward flow occupied the whole water column above 1000 m depth and extended to more than 80 km offshore~~) at this latitude.

The elevated poleward velocities ~~at the eastern boundary~~ were most likely ~~associated with~~caused by a ~~passing~~downwelling

510 CTW. Satellite SLA data ~~indicated a poleward propagation of~~indicate a positive ~~SLA signal~~anomaly propagating eastward from the ~~equator~~eastern equatorial Pacific to the South American coast and subsequently poleward to beyond 14° S. An elevated westerly wind anomaly on the equator in the central Pacific that occurred ~~simultaneously to the increase of poleward flow at 12° S.~~in April 2017 is suggested to have excited the initial Kelvin wave. Wind stress and wind stress curl variability along the South American coast did not impact the CTW nor the elevated alongshore velocities. The ~~SLA signal propagated~~

515 ~~at a speed consistent with the~~ phase speed of the SLA signal propagation along the South American coast is consistent with a first vertical mode CTW. Similarly, the vertical distribution of the poleward velocity anomaly at the eastern boundary ~~was consistent~~generally agreed with the cross-shore-depth velocity structure of a first ~~vertical~~ mode CTW.

~~Previous~~While temperature and salinity conditions remained almost unaltered, the enhanced poleward water mass advection due to the CTW induced changes in the distribution of oxygen and nutrient along the eastern boundary. Below 100m depth,

520 oxygen concentrations increased and the upper boundary of anoxic water ($O_2 > 2$ µmol kg⁻¹) deepened by about 50m due to both, the downward displacement of the isopycnals in the thermocline and the advection of ESSW having higher oxygen concentrations. Similarly, nitrate concentrations increased during the period of intensified poleward flow while phosphate concentrations and nitrogen deficit decreased (Fig. 12).

13

525 Similar to our results, previous studies have identified the first vertical mode CTWs to dominate intraseasonal variability in the eastern South Pacific based on tide gauge and SLA observations (e.g. Brink, 1982; Shaffer et al., 1997) and model results (Illig et al., 2018b). However, there is disagreement in the details of the observed ~~intraseasonal intensification of poleward flow within the~~ cross-shore-depth ~~range~~alongshore velocity structure of the ~~PCUC in a previous study by Pietri et al. (2014) was attributed to the second and third mode~~ CTW ~~modes. They found poleward velocities along~~and the ~~Peruvian continental slope increasing to 0.4 m s⁻¹.~~velocity structure of first vertical mode solution of a linear wave model using local stratification

530 and topography suggesting that additional dynamical processes are important.

~~Although the observed cross-shore-depth velocity structure of the CTW generally agrees with the first vertical mode solution of a linear wave model using local stratification and topography, there is disagreement in the details of the flow structure. It was noted previously that observed velocity structures agree poorly (Brink, 1982). Additionally, we compare only the theoretical modal structures with the difference between two velocity phases and the initial phase is no solid estimate of the~~

535 ~~mean alongshore circulation off Peru. Another possible explanation of the poor agreement between the first mode CTW and the observed flow intensification~~A possible explanation of the poor agreement is interaction of the CTW with local topography. North of our sampling site, the continental slope bends offshore at depths between 500 m to 1000 m (Fig. 1, insert) while the shelf narrows to the south. Changes in coastline, shelf width, and along-slope bathymetry lead to a transfer of CTW energy into higher modes (scattering) and upstream backscattering (Wang, 1980; Wilkin and Chapman, 1990; Kämpf~~(,~~ 2018~~);;~~

540 Brunner et al., 2019). The influence of changes in shelf width on the upstream alongshore flow structure can extend to 200 km upstream (Wilkin and Chapman, 1990) ~~and~~ but, due to relative smooth downstream topography, is likely not relevant here. However, the bent of the continental slope and other topographic irregularities north of ~~out~~our sampling site may stimulate energy transfer into high vertical mode CTWs. In turn, the superposition of several vertical modes could explain the observed elevated poleward flow between 50 m and 300 m depth~~.~~ (Fig. 3 and 12) that cannot be explained by a first mode CTW. In fact,

545 a recent model study suggests that differences between the theoretical CTW solutions and observations are predominately due to wave scattering (Brunner et al., 2019).

~~Furthermore, a recent study suggests that differences between the theoretical CTW solutions and observations are due to wave scattering into a greater proportion of higher-order modes or backscattering upstream (Brunner et al., 2019). Scattering occurs when a propagating CTW encounters changes in coastline, shelf width, and bathymetry. These changes were neglected when~~

550 ~~deriving the CTW mode solutions used here.~~

~~The SLA data indicate that the first vertical CTW mode along the eastern boundary that arrived at our sampling site in mid-May originated in the eastern equatorial Pacific at around 95° W (Fig. 6). A coherent signal from this region propagated eastwards along the equator and arrived at about the same time when the equatorial SLA maximum at the coast was developing. The wind data shows a possible forcing of this wave around 160° W in early April by a weakening of zonal wind (Fig. 7a).~~

555 ~~This is consistent with a recent comprehensive study (Rydbeck et al., 2019) identifying wind forcing variability west of 150° W as the main generation mechanism of intraseasonal equatorial Kelvin waves.~~

~~However, in the SLA the wave has an expression on east of 95° W compared to 150° W where Rydbeck et al. (2019) have located the maximum of SLA signal. The location of the SLA signal to the eastern equatorial Pacific may have been caused by the negative SLA further in the west which reduces the positive SLA to an extent where it is no longer identifiable.~~

560 The temperature and salinity conditions on the shelf remain almost unchanged despite the strongly intensified poleward flow ~~and are only displaced downwards~~, suggesting that the same water mass was advected within the boundary current regime during both observational periods. ~~The weak warming and increase in salinity agree with~~However, during the ~~advection~~presence of the ~~slightly warmer and saltier water along~~ CTW, SSTs were lower than in the ~~PCUC path north of 12° S (Grados et al., 2018). However, the signals are rather weak therefore we cannot relate them clearly~~period prior to the ~~circulation~~

565 ~~change. The SST declines despite the~~ wave. This is a somewhat unexpected result because downwelling ~~wave~~CTW weaken coastal upwelling due to the downward displacement of the thermocline which ~~would be expected to cause warming. A~~

14

~~downwelling CTW~~should lead to warmer SSTs and earlier in March 2017 ~~indeed has~~ downwelling CTWs contributed to the ~~warm SST anomalies~~anomalously high SST in the coastal El Niño (Echevin et al., 2018; Peng et al., 2019). However, previous studies have shown that the impact of CTWs on intraseasonal SST variability off Peru is limited ~~in general~~ (Dewitte et al.,

570 2011; Illig et al., 2014). Specifically, in May 2017 SST reduction agrees with both the seasonal cycle (Graco et al., 2017) and the decline of the warm Coastal El Niño with peak SST in March (e.g. Garreaud, 2018).

~~Despite being non-conservative, the changes~~Changes in oxygen concentrations ~~are small as well. Only in the bottom water on the upper continental slope, higher~~due to the CTW event were rather small. In the water column between 100 m and 200 m depth, oxygen concentrations ~~are displaced downwards. Faster advection should cause higher oxygen concentrations, because~~

575 ~~the time is shorter, in which oxygen is consumed by respiration along the PCUC path. Espinoza Morriberón et al. (2019) attribute some of the oxygen variability associated with El Niño Southern Oscillation to the changes in microbial respiration because advection speed and pathways change under El Niño conditions (e.g. Montes et al., 2011; Espinoza Morriberón et al., 2017).~~increased by 1 to 10 µmol kg^{-1}, only. However, ~~Zamora et al. (2012) reported uniform oxygen concentrations for waters in the PCUC; therefore, there is no oxygen change due to changes in alongshore advection, explaining the weak oxygen change~~

580 ~~in our study.~~

~~The~~the limited impact of the CTW on ~~the~~ oxygen ~~may be~~distribution is likely related to high oxygen concentrations present at the study site before the wave passage. ~~Compared to time series data of Callao (~~Previous measurement programs in this area found the mean depth of the upper boundary of the OMZ on the shelf at about 50 m depth (Gutiérrez et al., 2008; Dale et al., 2015, Graco et al., ~~2017) the concentrations were in the upper range of variability observed after the 1997-98 El Niño event.~~

585 ~~The 22 µmol kg^{-1} surface was located at 50 m instead of 30 m reported for the climatological state by Espinoza Morriberón et al. (2019). Whether the higher oxygen concentrations are caused by the coastal El Niño event, in the same way that canonical El Niños are related to enhanced oxygenation (e.g. Helly and Levin, 2004; Stramma et al., 2016; Espinoza Morriberón et al., 2019), cannot be answered with our available observational data. Coastal time series off northern Peru show an oxygenation starting in February 2017 but only a weaker signal at 12° S (ENFEN, 2017) while hydrographic profiles collected in early to~~

590 ~~mid-April at 11 and 14° S feature a very shallow oxycline (not shown). Therefore, it remains unclear whether the higher oxygen concentrations in late-April and May at 12° S are a local or short-term phenomenon or indeed related to the coastal El Niño event.~~2017) but deepening to 200 m or more during ENSO years (e.g. Levin et al., 2002; Espinoza-Morriberón et al., 2019). In particular, Dale et al. (2015) found oxygen levels below the detection limit between 30 and 400 m depth during previous measurement programs along 12° S. It is thus likely that the prevailing elevated

595 oxygen concentrations are related to the Coastal El Niño event in the same way that canonical El Niños are related to enhanced oxygenation (Helly and Levin, 2004; Espinoza-Morriberón et al., 2019). Despite small oxygen concentration changes, the upper boundary of anoxic water deepened by about 50 m during the presence of the CTW (Fig. 12). The change from anoxic conditions to suboxic conditions with oxygen concentrations (O_2 > 2 µmol kg^{-1}) has important consequences for biogeochemical processes and the benthic and pelagic communities (e.g. Gutiérrez et al., 2008). This study thus confirms

600 previous suggestions that CTW lead to episodic oxygenation events that are vital for colonization of invertebrates and other biota within the predominately anoxic regions of the benthos and the water column above.

The increase in nitrate concentrations and the reduced nitrogen deficit are likely caused by the ~~shorter~~faster advection ~~timescales in~~during the intensified flow period. The nitrate concentrations in the ESSW increase ~~occurs within the ESSW range~~ and waters with the same T-S properties are richer in nitrate ~~after the PCUC~~following the intensification of the PCUC

605 (Fig. 10), indicating the nitrate increase ~~(Fig. 9), excluding changed advection pathways as a likely cause of the increased nitrate load~~was not due to a different source of advected water. Along the ESSW pathway within the PCUC from the equator to 12° S, the nitrogen deficit increases while nitrate concentrations decrease (Silva et al., 2009; Zamora et al., 2012; Kalvelage et al., 2013~~). The increasing nitrogen deficit is caused by the microbially facilitated reduction of nitrate, nitrite and ammonium to N$_2$ gas which occurs in anoxic waters during the consumption of organic matter (e.g. Kalvelage et al., 2013~~). The resulting

nitrogen deficit accumulates with time during the poleward advection. Thus, ~~the~~an intensified PCUC increases the poleward advection of water with a lower nitrogen deficit. ~~The possibility of this mechanism is tested~~This can be verified by ~~calculating~~investigating the advection timescales ~~from the equatorial regime: the 12° S section is about 1800 km~~. The alongshore distance ~~away~~from the equator~~,~~ to the ~~advection timescale for~~12° S (1800 km) and a PCUC velocity of 0.4 m s⁻¹ ~~is~~yields a time scale of 52 days, ~~compared to~~while a time scale of 160 days ~~for~~results from a velocity of 0.13 m s⁻¹~~,~~ ~~approximately the~~representing maximum climatological ~~PCUC~~velocity (Chaigneau et al., 2013). Using ~~an~~a rate for N-loss of 48 nmol N l⁻¹~~d⁻¹~~ d⁻¹ (combined anammox and denitrification rates in the coastal OMZ from Kalvelage et al. ~~(2013)),~~(2013)) results in an N-loss difference of 5.2 µmol N l⁻¹ ~~can be transformed during the longer advection timescale. This may explain~~ due to the lower flow velocities. Indeed, the reduction of the nitrogen deficit by about 5 µmol N kg⁻¹, as observed throughout much of the PCUC core~~.~~ during the presence of the CTW, closely relates to this estimate. The sediments off Peru ~~below the OMZ~~subjected to oxygen depleted bottom waters, release phosphate into the water column (Noffke et al., 2012; Lomnitz et al., 2016) that also contributes to the nitrogen deficit. ~~Shorter~~Faster advection ~~timescales lead~~leads to a reduced accumulation of ~~benthic~~phosphate ~~release and in fact~~that is released from the sediments with lower phosphate concentrations ~~decrease~~ during the strong PCUC flow. However, the increase of nitrate ~~(and the sum of inorganic nitrogen species)~~exceeds the phosphate decrease by about 5 to 0.1 µmol kg⁻¹, a ratio higher than the nitrogen to phosphorus ~~relation implied~~ratio given in equation 1. Therefore, changes of nitrate concentration dominate the reduction of the nitrogen deficit.

The increase ~~of~~in nitrate by the downwelling CTW implies that the change ~~of~~in alongshore advection with the increased flow is more important for the nitrate balance than downwelling. The downwelling would displace the nutricline and thus transfer low nutrient surface ~~water~~waters downwards, lowering nutrient concentrations, which ~~is~~was not observed. The decline ~~of~~in nitrate concentrations during El Niño events has been associated with ~~the~~a nutricline displacement due to downwelling CTWs on interannual timescales (Graco et al., 2017; Espinoza-Morriberón et al., 2017). However, focusing on intraseasonal timescales, Echevin et al. (2014) modelled an almost cancelling of horizontal and vertical (i.e. nutricline movement) advection and a fast mode CTW not impacting nutricline depth. In a model study in the Atlantic Ocean, where nitrate decreases poleward as well, it was shown that the total effect of CTWs on nitrate concentrations varies regionally due to a different balance of horizontal and vertical advection ~~(Bachèlery et al., 2016),~~, but the horizontal advection always led to an increase in nitrate~~.~~ (Bachèlery et al., 2016).

The changes in redox state in the water column and especially ~~the~~bottom ~~water~~waters affect the biogeochemical cycling in the sediment as well. Because microbial storage of nitrate and nitrite by microorganisms in the sediment can sustain vigorous N turnover even in the absence of bottom water nitrate and nitrite (Dale et al., 2016; Sommer et al., 2016), episodic events of nitrogen supply can be associated with continuous benthic nitrogen cycling. The absence of nitrate supply due to the absence of CTWs over longer time periods favours the depletion of nitrate in the water column as observed by Sommer et al. (2016) and may lead ultimately to the development of sulfidic events (Schunck et al., 2013; Dale et al., ~~2017~~2016; Callbeck et al., 2018).

6 Conclusion

Based on extensive physical and biogeochemical sampling, we describe and analyse the evolution of circulation, hydrography and biogeochemistry off Peru in ~~early~~2017. Poleward velocities within the PCUC intensified ~~far beyond~~in May 2017 to several times the reported climatological mean ~~in May~~. This increased flow occurs during a limited time period in May in between weaker poleward transport in April and late June. The propagation velocity of positive SLA along the equator and coastline suggests that the intensified current is caused by a poleward propagating downwelling CTW of the first baroclinic mode forced around 160° W at the equator that ~~causes~~caused a positive SLA signal east of 95° W. The transition of the circulation from a

650 weak poleward flow to strong poleward flow decreased the timescale of alongshore advection from the equatorial current regime to the study site at 12° S.

The downwelling CTW is not associated with strong vertical displacements of waters; instead the advection caused by the intensified PCUC is more important. For parameters without strong horizontal gradients, an increase in PCUC flow does not cause pronounced changes in the advection. In this study this ~~applies~~applied to the conservative properties of temperature and

655 salinity as well as for oxygen where alongshore gradients are weak (Zamora et al., 2012). For these parameters there are no large differences between both circulation phases that can be attributed clearly to the altered circulation. Yet concentrations of nutrients are influenced by shorter transit times, being less altered by biogeochemical cycling. ~~Thisleads~~This leads to an increase of bioavailable nitrogen in the OMZ~~.~~ (Fig. 12) and its biogeochemistry is strongly changed by the increased ratio of nitrogen to phosphorus related to the increased advection~~.~~.

660 For the period from April to May 2017, our study suggests an increase in nitrate levels due to the passage of an intraseasonal downwelling CTW. This contrasts with the decrease observed previously on interannual timescales caused by downwelling CTWs (Graco et al., 2017). This shows that the impact of CTWs on nutrient biogeochemistry is a complex balance between different factors, with potentially different outcome on different timescales. Analysing the processes associated with individual intraseasonal waves is also necessary to understand the interannual effect of CTWs, which is based on varying occurrence of

665 such waves in different years.

The high variability of circulation, nutrients and the nitrogen deficit demonstrates the need for temporally resolved sampling as an individual section recorded may be very different from the situation a few weeks later. Quantification of intraseasonal variability in CTWs and their impact is – other than in modelling studies (e.g. Echevin et al., 2014) – only possible by sampling at high temporal resolution.

References

Albert, A., Echevin, V., Lévy, M., and Aumont, O.: Impact of nearshore wind stress curl on coastal circulation and primary productivity in the Peru upwelling system, J. Geophys. Res. Oceans, 115. doi:10.1029/2010JC006569, 2010.

695   Bachèlery, M.-L., Illig, S., and Dadou, I.: Forcings of nutrient, oxygen, and primary production interannual variability in the southeast Atlantic Ocean, Geophys. Res. Lett., 43, 8617-8625. doi:10.1002/2016gl070288, 2016.

Bakun, A. and Nelson, C. S.: The Seasonal Cycle of Wind-Stress Curl in Subtropical Eastern Boundary Current Regions, J. Phys. Oceanogr., 21, 1815-1834. doi:10.1175/1520-0485(1991)021<1815:TSCOWS>2.0.CO;2, 1991.

Becker, J. J., Sandwell, D. T., Smith, W. H. F., Braud, J., Binder, B., Depner, J., Fabre, D., Factor, J., Ingalls, S., Kim, S.-H.,
700   Ladner, R., Marks, K., Nelson, S., Pharaoh, A., Trimmer, R., Rosenberg, J. V., Wallace, G. and Weatherall, P.: Global Bathymetry and Elevation Data at 30 Arc Seconds Resolution: SRTM30_PLUS, Marine Geodesy, 32(4), 355–371, doi:10.1080/01490410903297766, 2009.

Belmadani, A., Echevin, V., Dewitte, B., and Colas, F.: Equatorially forced intraseasonal propagations along the Peru-Chile coast and their relation with the nearshore eddy activity in 1992–2000: A modeling study, J. Geophys. Res. Oceans, 117.
705   doi:10.1029/2011JC007848, 2012.

Bentamy, A. and Fillon, D. C.: Gridded surface wind fields from Metop/ASCAT measurements, Int. J. Remote Sens., 33, 1729-1754. doi:10.1080/01431161.2011.600348, 2012.

Brandt, P., Bange, H. W., Banyte, D., Dengler, M., Didwischus, S.-H., Fischer, T., Greatbatch, R. J., Hahn, J., Kanzow, T., Karstensen, J., Körtzinger, A., Krahmann, G., Schmidtko, S., Stramma, L., Tanhua, T., and Visbeck, M.: On the role of
710   circulation and mixing in the ventilation of oxygen minimum zones with a focus on the eastern tropical North Atlantic, Biogeosciences, 12, 489-512. doi:10.5194/bg-12-489-2015, 2015.

Brink, K. H.: A Comparison of Long Coastal Trapped Wave Theory with Observations off Peru, J. Phys. Oceanogr., 12, 897-913. doi:10.1175/1520-0485(1982)012<0897:ACOLCT>2.0.CO;2, 1982.

Brink, K. H.: Energy Conservation in Coastal-Trapped Wave Calculations, J. Phys. Oceanogr., 19, 1011-1016.
715   doi:10.1175/1520-0485(1989)019<1011:ECICTW>2.0.CO;2, 1989.

Brink, K. H.: Stable coastal-trapped waves with stratification, topography and mean flow, MBLWHOI Library. doi:10.1575/1912/10527, 2018.

Brink, K. H. and Chapman, D. C.: Programs for computing properties of coastal-trapped waves and wind-driven motions over the continental shelf and slope, WHOI Technical Reports, Woods Hole Oceanographic Institution. doi:10.1575/1912/5368,
720   1987.

Brink, K. H., Halpern, D. and Smith, R. L.: Circulation in the Peruvian upwelling system near 15°S, J. Geophys. Res., 85(C7), 4036–4048, doi:10.1029/jc085ic07p04036, 1980.

Brink, K. H., Halpern, D., Huyer, A., and Smith, R. L.: The physical environment of the Peruvian upwelling system, Prog. Oceanogr., 12, 285-305. doi:10.1016/0079-6611(83)90011-3, 1983.

725   Brunner, K., Rivas, D. and Lwiza, K. M. M.: Application of Classical Coastal Trapped Wave Theory to High-Scattering Regions, J. Phys. Oceanogr., 49(9), 2201–2216, doi:10.1175/JPO-D-18-0112.1, 2019.

Callbeck, C. M., Lavik, G., Ferdelman, T. G., Fuchs, B., Gruber-Vodicka, H. R., Hach, P. F., Littmann, S., Schoffelen, N. J., Kalvelage, T., Thomsen, S., Schunck, H., Löscher, C. R., Schmitz, R. A., and Kuypers, M. M. M.: Oxygen minimum zone cryptic sulfur cycling sustained by offshore transport of key sulfur oxidizing bacteria, Nat. Commun., 9. doi:10.1038/s41467-

730   018-04041-x, 2018.

Carr, M.-E.: Estimation of potential productivity in Eastern Boundary Currents using remote sensing, Deep Sea Res. Part II, 49, 59-80. doi:10.1016/S0967-0645(01)00094-7, 2002.

Chaigneau, A., Dominguez, N., Eldin, G., Vasquez, L., Flores, R., Grados, C., and Echevin, V.: Near-coastal circulation in the Northern Humboldt Current System from shipboard ADCP data, J. Geophys. Res. Oceans, 118, 5251-5266.

735   doi:10.1002/jgrc.20328, 2013.

Chang, B. X., Devol, A. H., and Emerson, S. R.: Denitrification and the nitrogen gas excess in the eastern tropical South Pacific oxygen deficient zone, Deep Sea Res. Part I, 57, 1092-1101. doi:10.1016/j.dsr.2010.05.009, 2010.

Chavez, F. P., Bertrand, A., Guevara-Carrasco, R., Soler, P., and Csirke, J.: The northern Humboldt Current System: Brief history, present status and a view towards the future, Prog. Oceanogr., 79, 95-105. doi:10.1016/j.pocean.2008.10.012, 2008.

740   Codispoti, L. A.: An oceanic fixed nitrogen sink exceeding 400 Tg N a^{-1} vs the concept of homeostasis in the fixed nitrogen inventory, Biogeosciences, 4, 233-253. doi:10.5194/bg-4-233-2007, 2007.

Colas, F., Capet, X., McWilliams, J. C. and Shchepetkin, A.: 1997-1998 El Niño off Peru: A numerical study, Prog. Oceanogr., 79(2-4), 138-155, doi:10.1016/j.pocean.2008.10.015, 2008.

Cornejo-Rodriguez, M. D. P. and Enfield, D. B.: Propagation and forcing of high-frequency sea level variability along the

745   west coast of South America, J. Geophys. Res. Oceans, 92(C13), 14323-14334, doi:10.1029/JC092iC13p14323, 1987.Czeschel, R., Stramma, L., Schwarzkopf, F. U., Giese, B. S., Funk, A., and Karstensen, J.: Middepth circulation of the eastern tropical South Pacific and its link to the oxygen minimum zone, J. Geophys. Res. Oceans, 116. doi:10.1029/2010JC006565, 2011.

Dale, A. W., Graco, M., and Wallmann, K.: Strong and Dynamic Benthic-Pelagic Coupling and Feedbacks in a Coastal

750   Upwelling System (Peruvian Shelf), Front. Mar. Sci. 4:29, doi.org/10.3389/fmars.2017.00029, 2017.

Dale, A. W., Sommer, S., Lomnitz, U., Montes, I., Treude, T., Liebetrau, V., Gier, J., Hensen, C., Dengler, M., Stolpovsky, K., Bryant, L. D. and Wallmann, K.: Organic carbon production, mineralisation and preservation on the Peruvian margin, Biogeosciences, 12(5), 1537–1559, doi:10.5194/bg-12-1537-2015, 2015.

Dale, A. W., Sommer, S., Lomnitz, U., Bourbonnais, A., and Wallmann, K.: Biological nitrate transport in sediments on the

755   Peruvian margin mitigates benthic sulfide emissions and drives pelagic N loss during stagnation events, Deep Sea Res. Part I, 112, 123-136. doi:10.1016/j.dsr.2016.02.013, 2016.

Dengler, M. and Sommer, S.: Coupled benthic and pelagic oxygen, nutrient and trace metal cycling, ventilation and carbon degradation in the oxygen minimum zone of the Peruvian continental margin (SFB 754): Cruise No. M 136 11.04. - 03.05.2017 Callao (Peru) - Callao Solute-Flux Peru I, METEOR-Berichte, doi:10.3289/CR_M136, 2017.

760   DeVries, T., Deutsch, C., Rafter, P. A., and Primeau, F.: Marine denitrification rates determined from a global 3-D inverse model, Biogeosciences, 10, 2481-2496. doi:10.5194/bg-10-2481-2013, 2013.

Dewitte, B., Illig, S., Renault, L., Goubanova, K., Takahashi, K., Gushchina, D., Mosquera, K. and Purca, S.: Modes of covariability between sea surface temperature and wind stress intraseasonal anomalies along the coast of Peru from satellite observations (2000–2008), J. Geophys. Res. Oceans, 116(C4), doi:10.1029/2010JC006495, 2011.

765   Echevin, V., Albert, A., Lévy, M., Graco, M., Aumont, O., Piétri, A., and Garric, G.: Intraseasonal variability of nearshore productivity in the Northern Humboldt Current System: The role of coastal trapped waves, Cont. Shelf Res., 73, 14-30. doi:10.1016/j.csr.2013.11.015, 2014.

Echevin, V., Colas, F., Espinoza-Morriberon, D., Vasquez, L., Anculle, T., and Gutierrez, D.: Forcings and Evolution of the 2017 Coastal El Niño Off Northern Peru and Ecuador, Front. Mar. Sci., 5, 367. doi:10.3389/fmars.2018.00367, 2018.

770 ~~ENFEN: Technical Report ENFEN no 3 2017, Comité Multisectorial encargado del Estudio Nacional del Fenómeno El Niño (Enfen). [online] Available from: https://www.dhn.mil.pe/Archivos/oceanografia/enfen/informe-tecnico/03-2017.pdf, 2017.~~

Enfield, D. B., Cornejo-Rodriguez, M. D., Smith, R. L., and Newberger, P. A.: The equatorial source of propagating variability along the Peru coast during the 1982–1983 El Niño, J. Geophys. Res. Oceans, 92, 14335-14346. doi:10.1029/JC092iC13p14335, 1987.

775 Espinoza-Morriberón, D., Echevin, V., Colas, F., Tam, J., Gutierrez, D., Graco, M., Ledesma, J. and Quispe-Ccalluari, C.: Oxygen Variability During ENSO in the Tropical South Eastern Pacific, Front. Mar. Sci., 5, 526, doi:10.3389/fmars.2018.00526, 2019.

Espinoza-Morriberón, D., Echevin, V., Colas, F., Tam, J., Ledesma, J., Vásquez, L., and Graco, M.: Impacts of El Niño events on the Peruvian upwelling system productivity, J. Geophys. Res. Oceans. doi:10.1002/2016JC012439, 2017.

780 Fennel, W., Junker, T., Schmidt, M. and Mohrholz, V.: Response of the Benguela upwelling systems to spatial variations in the wind stress, Cont. Shelf Res., 45, 65–77, doi:10.1016/j.csr.2012.06.004, 2012.

Fischer, J., Brandt, P., Dengler, M., Müller, M., and Symonds, D.: Surveying the Upper Ocean with the Ocean Surveyor: A New Phased Array Doppler Current Profiler, J. Atmos. Oceanic Technol., 20, 742-751. doi:10.1175/1520-0426(2003)20<742:STUOWT>2.0.CO;2, 2003.

785 Garreaud, R. D.: A plausible atmospheric trigger for the 2017 coastal El Niño, Int. J. Climatol., 38, e1296-e1302. doi:10.1002/joc.5426, 2018.

Graco, M. I., Purca, S., Dewitte, B., Castro, C. G., Morón, O., Ledesma, J., Flores, G. and Gutiérrez, D.: The OMZ and nutrient features as a signature of interannual and low-frequency variability in the Peruvian upwelling system, Biogeosciences, 14(20), 4601–4617, doi:10.5194/bg-14-4601-2017, 2017.

790 Grados, C., Chaigneau, A., Echevin, V., and Dominguez, N.: Upper ocean hydrology of the Northern Humboldt Current System at seasonal, interannual and interdecadal scales, Prog. Oceanogr., 165, 123-144. doi:10.1016/j.pocean.2018.05.005, 2018.

Grasshoff, K., Kremling, K. and Ehrhardt, M.: Methods of seawater analysis, John Wiley & Sons., 1983.

Gruber, N.: The ~~Dynamics of the Marine Nitrogen Cycle~~marine nitrogen cycle: overview and ~~its Influence on Atmospheric~~
795 ~~CO2 Variations~~challenges, in ~~The Ocean Carbon Cycle and Climate~~Nitrogen in the marine environment, vol. 2, edited by D. G. Capone, D. A. Bronk, M. ~~Follows~~Mulholland, and E. J. ~~T. Oguz~~Carpenter, pp. ~~97–148, Springer Netherlands, Dordrecht., 2004~~1–50, Elsevier Amsterdam., 2008.

Gruber, N. and Sarmiento, J. L.: Global patterns of marine nitrogen fixation and denitrification, Global Biogeochem. Cycles, 11, 235-266. doi:10.1029/97GB00077, 1997

800 Gruber, N. and Sarmiento, J. L.: Large-scale biogeochemical-physical interactions in elemental cycles, in THE SEA: Biological–Physical Interactions in the Oceans, vol. 12, edited by A. R. Robinson, J. J. McCarthy, and B. J. Rothschild, pp. 337–399, Wiley, New York., 2002.

Gunther, E. R.: A report on oceanographical investigations in the Peru Coastal Current, Discovery Rep., 13, 107–276, 1936.

Gutiérrez, D., Enríquez, E., Purca, S., Quipúzcoa, L., Marquina, R., Flores, G. and Graco, M.: Oxygenation episodes on the
805 continental shelf of central Peru: Remote forcing and benthic ecosystem response, Prog. Oceanogr., 79(2–4), 177–189, doi:10.1016/j.pocean.2008.10.025, 2008.

Hauschildt, J., Thomsen, S., Echevin, V., Oschlies, A., José, Y. S., Krahmann, G., Bristow, L. A. and Lavik, G.: The fate of upwelled nitrate off Peru shaped by submesoscale filaments and fronts, Biogeosci. Discuss., 1–32, doi:10.5194/bg-2020-112, in review, 2020.

810 Helly, J. J. and Levin, L. A.: Global distribution of naturally occurring marine hypoxia on continental margins, Deep Sea Res. Part I, 51, 1159-1168. doi:10.1016/j.dsr.2004.03.009, 2004.

Hill, A. E., Hickey, B. M., Shillington, F. A., Strub, P. T., Brink, K. H., Barton, E. D. and Thomas, A. C.: Eastern Ocean Boundaries, in The Seas: The Global Coastal Ocean, vol. 11, edited by A. R. Robinson and K. H. Brink, pp. 29–68, John Wiley, New York., 1998.

815 Holmes, R. M., Aminot, A., Kérouel, R., Hooker, B. A., and Peterson, B. J.: A simple and precise method for measuring ammonium in marine and freshwater ecosystems, Can. J. Fish. Aquat.Sci., 56, 1801-1808. doi:10.1139/f99-128, 1999.

Hood, E. M., Sabine, C. L. and Sloyan, B. M.: The GO-SHIP Repeat Hydrography Manual: a collection of expert reports and guidelines, Version 1, IOCCP Report 14., ICPO Publication Series 134., 2010.

Hormazabal, S., Shaffer, G., and Pizarro, O.: Tropical Pacific control of intraseasonal oscillations off Chile by way of oceanic
820 and atmospheric pathways, Geophys. Res. Lett., 29. doi:10.1029/2001GL013481, 2002.

Huang, B., Thorne, P. W., Banzon, V. F., Boyer, T., Chepurin, G., Lawrimore, J. H., Menne, M. J., Smith, T. M., Vose, R. S. and Zhang, H.-M.: NOAA Extended Reconstructed Sea Surface Temperature (ERSST), Version 5, doi:10.7289/V5T72FNM, 2017a.

Huang, B., Thorne, P. W., Banzon, V. F., Boyer, T., Chepurin, G., Lawrimore, J. H., Menne, M. J., Smith, T. M., Vose, R. S.
825 and Zhang, H.-M.: Extended Reconstructed Sea Surface Temperature, Version 5 (ERSSTv5): Upgrades, Validations, and Intercomparisons, J. Climate, 30(20), 8179–8205, doi:10.1175/JCLI-D-16-0836.1, 2017b.Huyer, A., Knoll, M., Paluszkiewicz, T., and Smith, R. L.: The Peru Undercurrent: a study in variability, Deep Sea Res., 38, Supplement 1, S247 S271. doi:10.1016/S0198-0149(12)80012-4, 1991.

Illig, S., Bachèlery, M.-L., and Cadier, E.: Subseasonal Coastal-Trapped Wave Propagations in the Southeastern Pacific and
830 Atlantic Oceans: 2. Wave Characteristics and Connection With the Equatorial Variability, J. Geophys. Res. Oceans, 123, 3942-3961. doi:10.1029/2017JC013540, 2018b.

Illig, S., Cadier, E., Bachèlery, M.-L., and Kersalé, M.: Subseasonal Coastal-Trapped Wave Propagations in the Southeastern Pacific and Atlantic Oceans: 1. A New Approach to Estimate Wave Amplitude, J. Geophys. Res. Oceans, 123, 3915-3941. doi:10.1029/2017JC013539, 2018a

835 Illig, S., Dewitte, B., Goubanova, K., Cambon, G., Boucharel, J., Monetti, F., Romero, C., Purca, S. and Flores, R.: Forcing mechanisms of intraseasonal SST variability off central Peru in 2000–2008, J. Geophys. Res. Oceans, 119(6), 3548–3573, doi:10.1002/2013JC009779, 2014.

IOC, SCOR and IAPSO: The international thermodynamic equation of seawater – 2010: Calculation and use of thermodynamic properties, edited by U. (english), Intergovernmental Oceanographic Commission., 2010.

840 Junker, T., Schmidt, M. and Mohrholz, V.: The relation of wind stress curl and meridional transport in the Benguela upwelling system, J. Mar. Syst., 143, 1–6, doi:10.1016/j.jmarsys.2014.10.006, 2015.

Kalvelage, T., Lavik, G., Lam, P., Contreras, S., Arteaga, L., Löscher, C. R., Oschlies, A., Paulmier, A., Stramma, L. and Löml:Kuypers, M. M.: Nitrogen cycling driven by organic matter export in the South Pacific oxygen minimum zone, Nat. Geosci., 6(3), 228–234, doi:10.1038/ngeo1739, 2013.

845 Kämpf, J.: On the Dynamics of Canyon-Flow Interactions, Journal of Marine Science and Engineering, 6(4), doi:10.3390/jmse6040129, 2018.

Kämpf, J. and Chapman, P.: Upwelling Systems of the World: A Scientific Journey to the Most Productive Marine Ecosystems, Springer, 2016.

Karstensen, J., Schütte, F., Pietri, A., Krahmann, G., Fiedler, B., Grundle, D., Hauss, H., Körtzinger, A., Löscher, C. R., Testor,
850 P., Vieira, N. and Visbeck, M.: Upwelling and isolation in oxygen-depleted anticyclonic modewater eddies and implications for nitrate cycling, Biogeosciences, 14(8), 2167–2181, doi:10.5194/bg-14-2167-2017, 2017.

Karstensen, J., Stramma, L., and Visbeck, M.: Oxygen minimum zones in the eastern tropical Atlantic and Pacific oceans, Prog. Oceanogr., 77, 331-350. doi:10.1016/j.pocean.2007.05.009, 2008.

Klenz, T., Dengler, M., and Brandt, P.: Seasonal Variability of the Mauritania Current and Hydrography at 18° N, J. Geophys. Res. Oceans, 123, 8122-8137. doi:10.1029/2018jc014264, 2018.

Kuypers, M. M. M., Lavik, G., Woebken, D., Schmid, M., Fuchs, B. M., Amann, R., Jørgensen, B. B. and Jetten, M. S. M.: Massive nitrogen loss from the Benguela upwelling system through anaerobic ammonium oxidation, Proceedings of the National Academy of Sciences, 102(18), 6478–6483, doi:10.1073/pnas.0502088102, 2005.

Lam, P., Lavik, G., Jensen, M. M., van de Vossenberg, J., Schmid, M., Woebken, D., Gutiérrez, D., Amann, R., Jetten, M. S. M. and Kuypers, M. M. M.: Revising the nitrogen cycle in the Peruvian oxygen minimum zone, Proceedings of the National Academy of Sciences, 106(12), 4752–4757, doi:10.1073/pnas.0812444106, 2009.

Leth, O. and Middleton, J. F.: A numerical study of the upwelling circulation off central Chile: Effects of remote oceanic forcing, J. Geophys. Res. Oceans, 111(C12), doi:10.1029/2005JC003070, 2006.

Lomnitz, U., Sommer, S., Dale, A. W., Löscher, C. R., Noffke, A., Wallmann, K., and Hensen, C.: Benthic phosphorus cycling in the Peruvian oxygen minimum zone, Biogeosciences, 13, 1367-1386. doi:10.5194/bg-13-1367-2016, 2016.

Levin, L., Gutiérrez, D., Rathburn, A., Neira, C., Sellanes, J., Muñoz, P., Gallardo, V. and Salamanca, M.: Benthic processes on the Peru margin: a transect across the oxygen minimum zone during the 1997–98 El Niño, Prog. Oceanogr., 53(1), 1–27, doi:10.1016/S0079-6611(02)00022-8, 2002.

Marchesiello, P., McWilliams, J. C. and Shchepetkin, A.: Equilibrium Structure and Dynamics of the California Current System, J. Phys. Oceanogr., 33(4), 753–783, doi: 10.1175/1520-0485(2003)33<753:ESADOT>2.0.CO;2, 2003.

McCreary, J. P. and Chao, S.-Y.: Three-dimensional shelf circulation along an eastern ocean boundary, J. Mar. Res., 43, 13-36. doi:10.1357/002224085788437316, 1985.

McCreary, J. P., Kundu, P. K. and Chao, S. Y.: On the dynamics of the California Current system, J. Mar. Res., 45(1), 1–32, doi:10.1357/002224087788400945, 1987.McDougall, T.McDougall, T. J. and Barker, P. M.: Getting started with TEOS-10 and the Gibbs Seawater (GSW) oceanographic toolbox, SCOR/IAPSO WG 127, 2011.

Montes, I., Colas, F., Capet, X., and Schneider, W.: On the pathways of the equatorial subsurface currents in the eastern equatorial Pacific and their contributions to the Peru-Chile Undercurrent, J. Geophys. Res. Oceans, 115. doi:10.1029/2009JC005710, 2010.

Montes, I., Schneider, W., Colas, F., Blanke, B., and Echevin, V.: Subsurface connections in the eastern tropical Pacific during La Niña 1999–2001 and El Niño 2002–2003, J. Geophys. Res. Oceans, 116. doi:10.1029/2011JC007624, 2011.

Moore, D. W. and Philander, S. G. H.: Modelling of the tropical ocean circulation, in The Sea, vol. 6, pp. 316–361, John Wiley., 1977.

Noffke, A., Hensen, C., Sommer, S., Scholz, F., Bohlen, L., Mosch, T., Graco, M. and Wallmann, K.: Benthic iron and phosphorus fluxes across the Peruvian oxygen minimum zone, Limnol. Oceanogr., 57(3), 851–867, doi:10.4319/lo.2012.57.3.0851, 2012.

Paulmier, A. and Ruiz Pino, D.: Oxygen minimum zones (OMZs) in the modern ocean, Prog. Oceanogr., 80, 113–128. doi:10.1016/j.pocean.2008.08.001, 2009.

Pennington, J. T., Mahoney, K. L., Kuwahara, V. S., Kolber, D. D., Calienes, R., and Chavez, F. P.: Primary production in the eastern tropical Pacific: A review, Prog. Oceanogr., 69, 285-317. doi:10.1016/j.pocean.2006.03.012, 2006.

Penven, P., Echevin, V., Pasapera, J., Colas, F., and Tam, J.: Average circulation, seasonal cycle, and mesoscale dynamics of the Peru Current System: A modeling approach, J. Geophys. Res. Oceans, 110. doi:10.1029/2005JC002945, 2005.

Philander, S. G. H. and Yoon, J.-H.: Eastern Boundary Currents and Coastal Upwelling, J. Phys. Oceanogr., 12(8), 862–879, doi:10.1175/1520-0485(1982)012<0862:EBCACU>2.0.CO;2, 1982.

Pietri, A., Echevin, V., Testor, P., Chaigneau, A., Mortier, L., Grados, C., and Albert, A.: Impact of a coastal-trapped wave on the near-coastal circulation of the Peru upwelling system from glider data, J. Geophys. Res. Oceans, 119, 2109-2120. doi:10.1002/2013JC009270, 2014.

Pizarro, O., Shaffer, G., Dewitte, B., and Ramos, M.: Dynamics of seasonal and interannual variability of the Peru-Chile Undercurrent, Geophys. Res. Lett., 29, 22-1 - 22-4. doi:10.1029/2002GL014790, 2002.

Ramos, M., Dewitte, B., Pizarro, O., and Garric, G.: Vertical propagation of extratropical Rossby waves during the 1997-1998 El Niño off the west coast of South America in a medium resolution OGCM simulation, J. Geophys. Res., 113. doi:10.1029/2007jc004681, 2008.

Revsbech, N. P., Larsen, L. H., Gundersen, J., Dalsgaard, T., Ulloa, O., and Thamdrup, B.: Determination of ultra-low oxygen concentrations in oxygen minimum zones by the STOX sensor, Limnol. Oceanogr. Methods, 7, 371-381. doi:10.4319/lom.2009.7.371, 2009.

Rydbeck, A. V., Jensen, T. G., Romea, R. D. and Flatau, M.: Characterization of Intraseasonal Kelvin Smith, R. L.: Further Evidence for Coastal Trapped Waves in along the Equatorial Pacific Ocean Peru Coast, J. Phys. Oceanogr., Geophys. Res. Oceans, 124, 2028 2053. 13(8), 1341–1356, doi:10.1029/2018jc014838, 2019 1175/1520-0485(1983)013<1341:FEFCTW>2.0.CO;2, 1983.

Sakamoto, C. M., Johnson, K. S., and Coletti, L. J.: Improved algorithm for the computation of nitrate concentrations in seawater using an in situ ultraviolet spectrophotometer, Limnol. Oceanogr. Methods, 7, 132-143. doi:10.4319/lom.2009.7.132, 2009.

Schunck, H., Lavik, G., Desai, D. K., Großkopf, T., Kalvelage, T., Löscher, C. R., Paulmier, A., Contreras, S., Siegel, H., Holtappels, M., Rosenstiel, P., Schilhabel, M. B., Graco, M., Schmitz, R. A., Kuypers, M. M. M. and LaRoche, J.: Giant Hydrogen Sulfide Plume in the Oxygen Minimum Zone off Peru Supports Chemolithoautotrophy, PLoS One, 8(8), 1–18, doi:10.1371/journal.pone.0068661, 2013.

Shaffer, G., Pizarro, O., Djurfeldt, L., Salinas, S., and Rutllant, J. (1997). Circulation and Low-Frequency Variability near the Chilean Coast: Remotely Forced Fluctuations during the 1991–92 El Niño, Journal of Physical Oceanography, 27, 217-235. doi:10.1175/1520-0485(1997)027<0217:CALFVN>2.0.CO;2, 1997.

Silva, N., Rojas, N., and Fedele, A.: Water masses in the Humboldt Current System: Properties, distribution, and the nitrate deficit as a chemical water mass tracer for Equatorial Subsurface Water off Chile, Deep Sea Res. Part II, 56, 1004-1020. doi:10.1016/j.dsr2.2008.12.013, 2009.

Sommer, S., Gier, J., Treude, T., Lomnitz, U., Dengler, M., Cardich, J., and Dale, A. W.: Depletion of oxygen, nitrate and nitrite in the Peruvian oxygen minimum zone cause an imbalance of benthic nitrogen fluxes, Deep Sea Res. Part I, 112, 113-122. doi:10.1016/j.dsr.2016.03.001, 2016.

Sommer, S., Dengler, M. and Shipboard Scientific Party.: Benthic element cycling, fluxes and transport of nutrients and trace metals across the benthic boundary layer in the Peruvian oxygen minimum zone (SFB 754), Cruise No. 137, 06.05. - 29.05.2017, Callao (Peru) - Callao, METEOR-Berichte, doi:10.2312/cr_m137, 2019.

Stramma, L., Fischer, T., Grundle, D. S., Krahmann, G., Bange, H. W., and Marandino, C. A.: Observed El Niño conditions in the eastern tropical Pacific in October 2015, Ocean Sci., 12, 861-873. doi:10.5194/os-12-861-2016, 2016.

Strub, P. T., Mesias, J. M., Montecino, V., Rutllant, J. and Salinas, S.: Coastal ocean circulation off western South America, in The Seas: The Global Coastal Ocean, vol. 11, edited by A. R. Robinson and K. H. Brink, pp. 273–313, John Wiley, New York., 1998.

Thomsen, S., Kanzow, T., Krahmann, G., Greatbatch, R. J., Dengler, M., and Lavik, G.: The formation of a subsurface anticyclonic eddy in the Peru-Chile Undercurrent and its impact on the near-coastal salinity, oxygen, and nutrient distributions, J. Geophys. Res. Oceans, 121, 476-501. doi:10.1002/2015JC010878, 2016.

Thomsen, S., Karstensen, J., Kiko, R., Krahmann, G., Dengler, M., and Engel, A.: Remote and local drivers of oxygen and nitrate variability in the shallow oxygen minimum zone off Mauritania in June 2014, Biogeosciences, 16, 979-998. doi:10.5194/bg-16-979-2019, 2019.

Thyng, K. M., Greene, C. A., Hetland, R. D., Zimmerle, H. M. and DiMarco, S. F.: True Colors of Oceanography: Guidelines

940   for Effective and Accurate Colormap Selection, Oceanography, 29, doi:10.5670/oceanog.2016.66, 2016.

Ulloa, O., Canfield, D. E., DeLong, E. F., Letelier, R. M. and Stewart, F. J.: Microbial oceanography of anoxic oxygen minimum zones, Proceedings of the National Academy of Sciences, 109(40), 15996–16003, doi:10.1073/pnas.1205009109, 2012.

Wang, D.-P.: Diffraction of Continental Shelf Waves by Irregular Alongshore Geometry, J. Phys. Oceanogr., 10(8), 1187–

945   1199, doi:10.1175/1520-0485(1980)010<1187:DOCSWB>2.0.CO;2, 1980.Wilkin, J. L. and Chapman, D. C.: Scattering of Coastal-Trapped Waves by Irregularities in Coastline and Topography, J. Phys. Oceanogr., W. L., Moore, J. K., Martiny, A. C. and Primeau, F. W.: Convergent estimates of marine nitrogen fixation, Nature, 566(7743), 205–211, doi:10.1038/s41586-019-0911-2, 201920(3), 396–421, doi:10.1175/1520-0485(1990)020<0396:SOCTWB>2.0.CO;2, 1990.

Winkler, L. W.: Die Bestimmung des im Wasser gelösten Sauerstoffes, Ber. Dtsch. Chem. Ges., 21(2), 2843–2854,

950   doi:10.1002/cber.188802102122, 1888.

H. Yoon, J.-H. and Philander, S. G. H.: The generation of coastal undercurrents, J. Oceanogr. Soc. Jpn., 38(4), 215–224, doi:10.1007/bf02111104, 1982.

Yu, X., and McPhaden, M. J.: Seasonal Variability in the Equatorial Pacific, J. Phys. Oceanogr., 29, 925-947. doi:10.1175/1520-0485(1999)029<0925:SVITEP>2.0.CO;2, 1999.

955   Zamora, L. M., Oschlies, A., Bange, H. W., Huebert, K. B., Craig, J. D., Kock, A., and Löscher, C. R.: Nitrous oxide dynamics in low oxygen regions of the Pacific: insights from the MEMENTO database, Biogeosciences, 9, 5007-5022. doi:10.5194/bg-9-5007-2012, 2012.

Zhang, W.and Lentz, S. J.: Wind-Driven Circulation in a Shelf Valley. Part I: Mechanism of the Asymmetrical Response to Along-Shelf Winds in Opposite Directions, J. Phys. Oceanogr., 47(12), 2927–2947, doi:10.1175/JPO-D-17-0083.1, 2017.

Table 1: Dates of R/V Meteor cruises conducted within the ETSP in 2017 including sampling time and number of CTD stations collected 12° S.

R/V Meteor cruise	Dates in 2017	Sampling duration along 12° S	CTD/nutrient stations at 12° S
M135	March 2 – April 8	2 days	
M136	April 18 – May 3	15 days	59 profiles
M137	May 6 – 29	23 days	92 profiles
M138	June 1 – July 5	1 day	
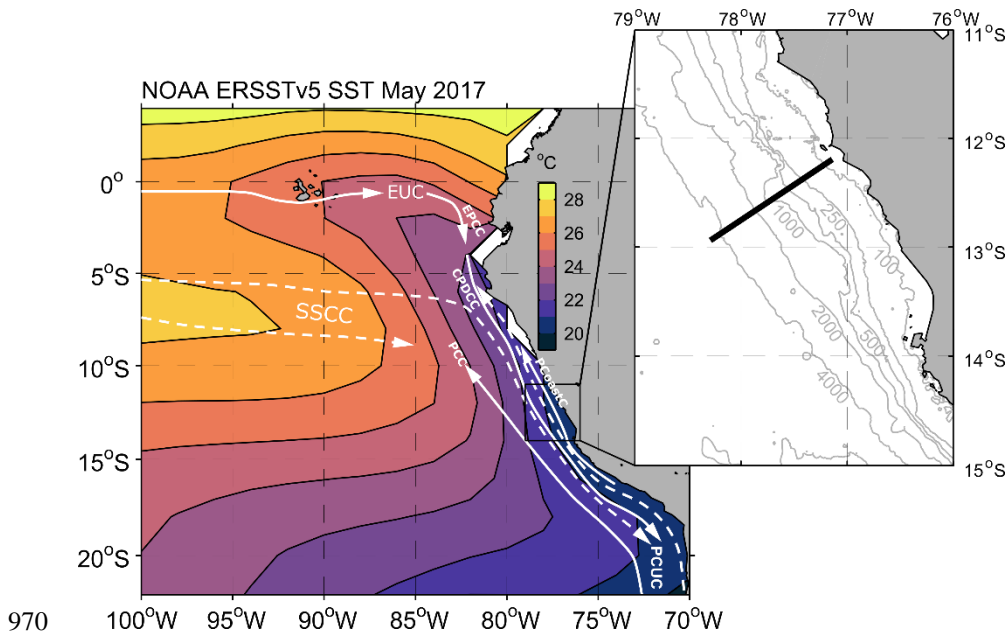
Figure 1: Sea surface temperature (NOAA ERSSTv5 SST) in the eastern tropical Pacific during May 2017 and schematic of the circulation. White solid lines indicate surface layer currents while dashed lines indicate thermocline layer currents (after Brandt et al., 2015). Abbreviated currents are the Equatorial Undercurrent (EUC), the Ecuador-Peru Coastal Current (EPCC), the Peru Coastal Current (PCoastC), the Peru Chile Current (PCC), the Southern Subsurface Countercurrents (SSCC, with two branches), the Chile–Peru Deep Coastal Current (CPDCC), and the Peru–Chile Undercurrent (PCUC). Figure insert shows the position of the 12° S section and local bathymetry (SRTM30 plus topography, Becker et al., 2009).
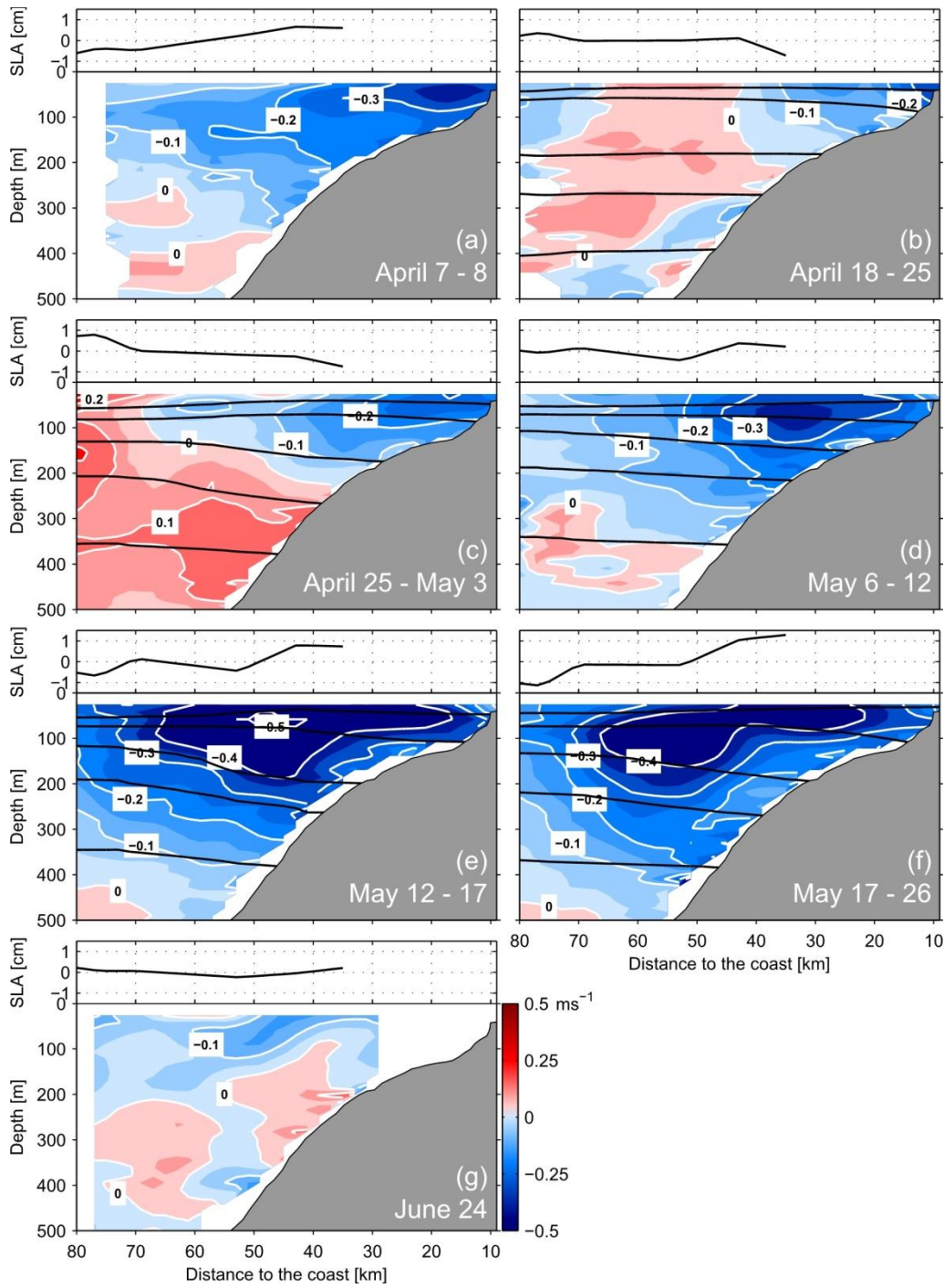
Figure 2: Depth-distance distribution of alongshore velocity (in m s⁻¹, positive equatorward, lower subpanels) and sea level anomaly (in cm, upper subpanels) at 12° S during April 7 – 8 (a), April 18 –25 (b), April 25 – May 3 (c), May 6 -12 (d), May 12 – 17 (e), May 17 – 26 (f) and June 24, 2017 (g). Black lines indicate the distribution of isopycnals (σ_θ) 25.6, 25.9, 26.2, 26.4, and 26.7 kg m⁻³.
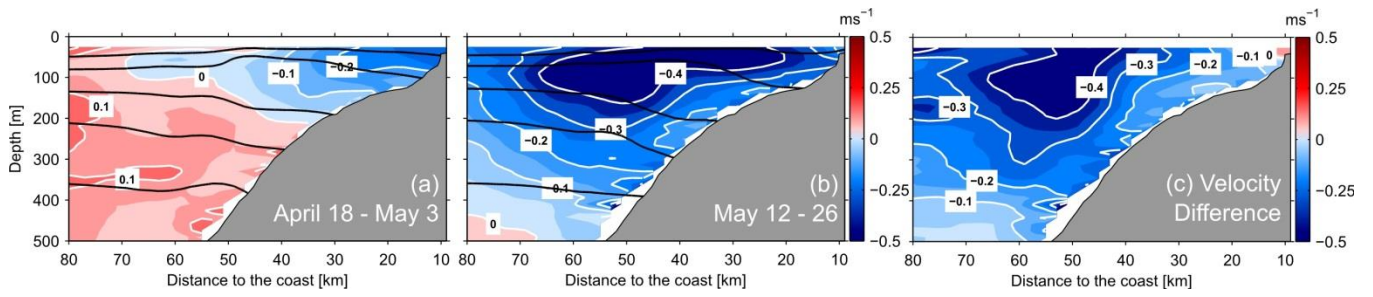
Figure 3: Depth - distance distribution of averaged alongshore velocity (positive equatorward) at 12° S prior to (a, April 18 – May 3, 2017) and during (b, May 12 – 26, 2017) the PCUC intensification period. Panel c depicts the velocity difference between the two situations. Black lines indicate the distribution of isopycnals (σ_θ) 25.6, 25.9, 26.2, 26.4, and 26.7 kg m⁻³.

1000
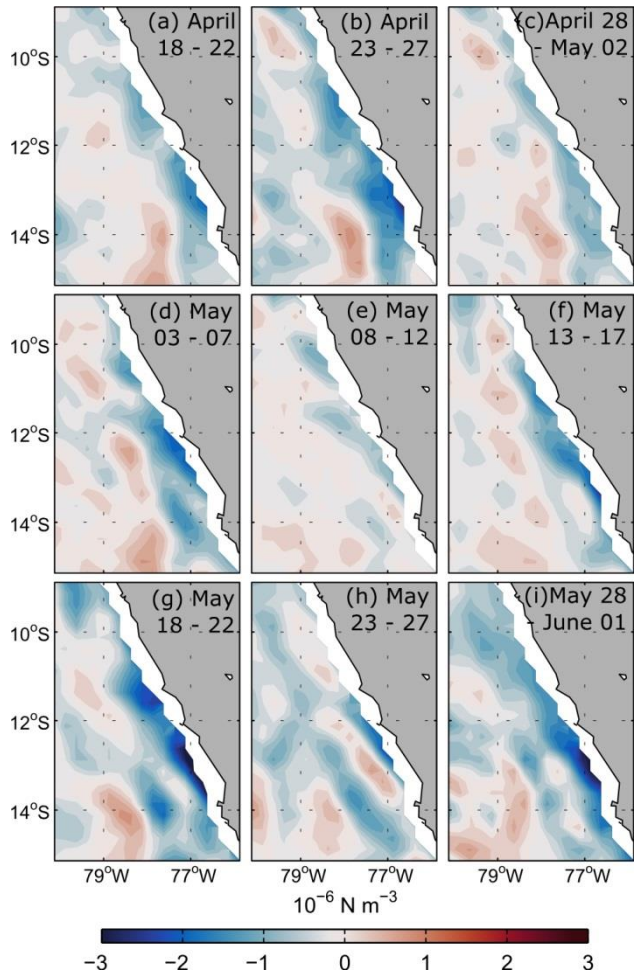
Figure 4: Five-day mean wind stress curl from ASCAT scatterometer winds off Peru during April 18 – 22 (a), April (23 – 27 (b),
April 28 – May 02 (c), May 03 – 07 (d), May 08 – 12 (e), May 13 – 17 (f), May 18 – 22 (g), May 23 – 27 (h) and May 28 – June 01,
2017 (i).
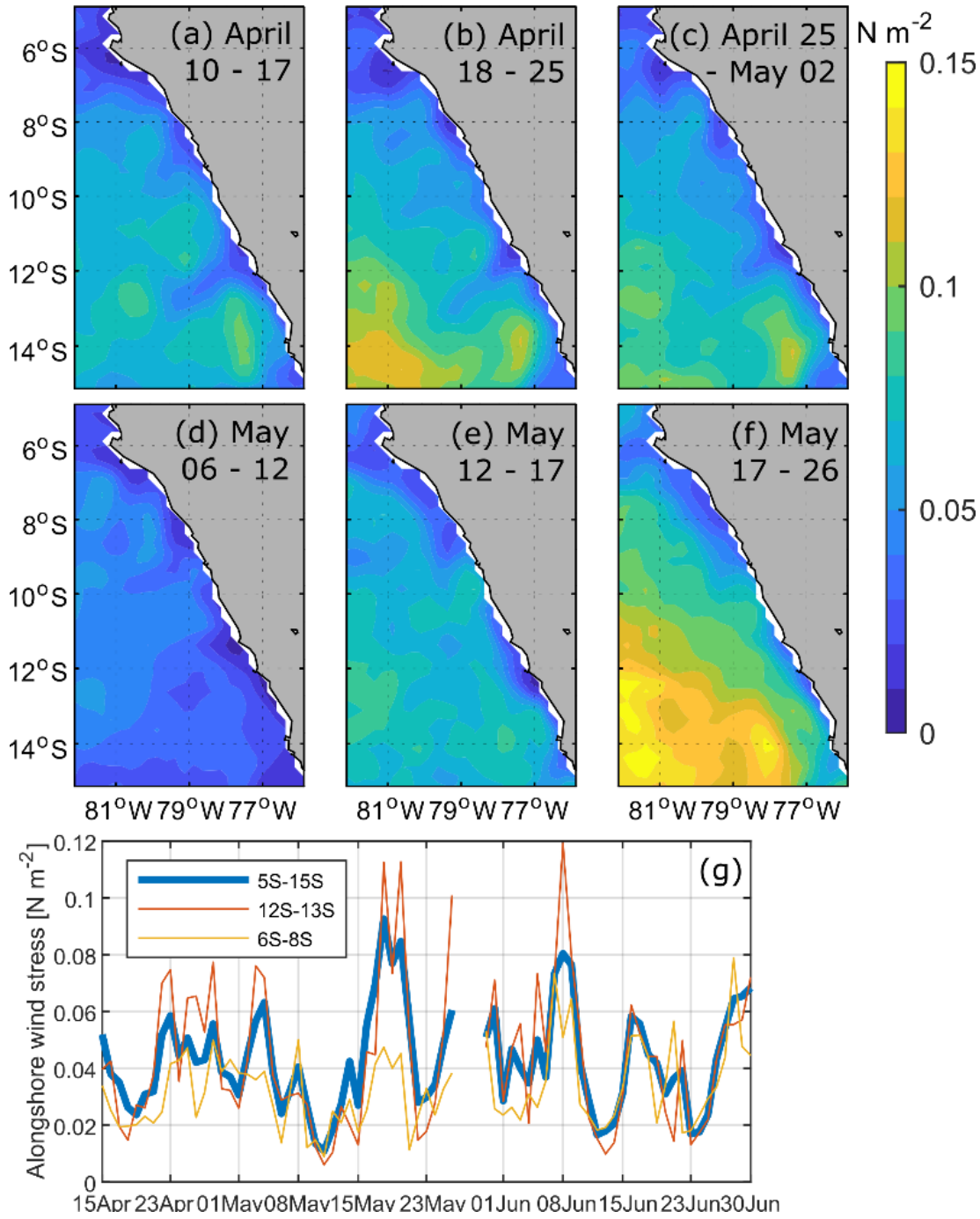
Figure 5: Weekly averages of alongshore wind stress from ASCAT scatterometer winds (upper two panel rows) for April 10 – 17 (a), April 18 -25 (b), April 25 – May 2 (c), May 06 – 12 (d), May 12 – 17 (e), May 17 – 26 (f). Lower panel (g) shows time series of alongshore wind stress averaged between 30 and 80 km from the coast for different bands of latitude.
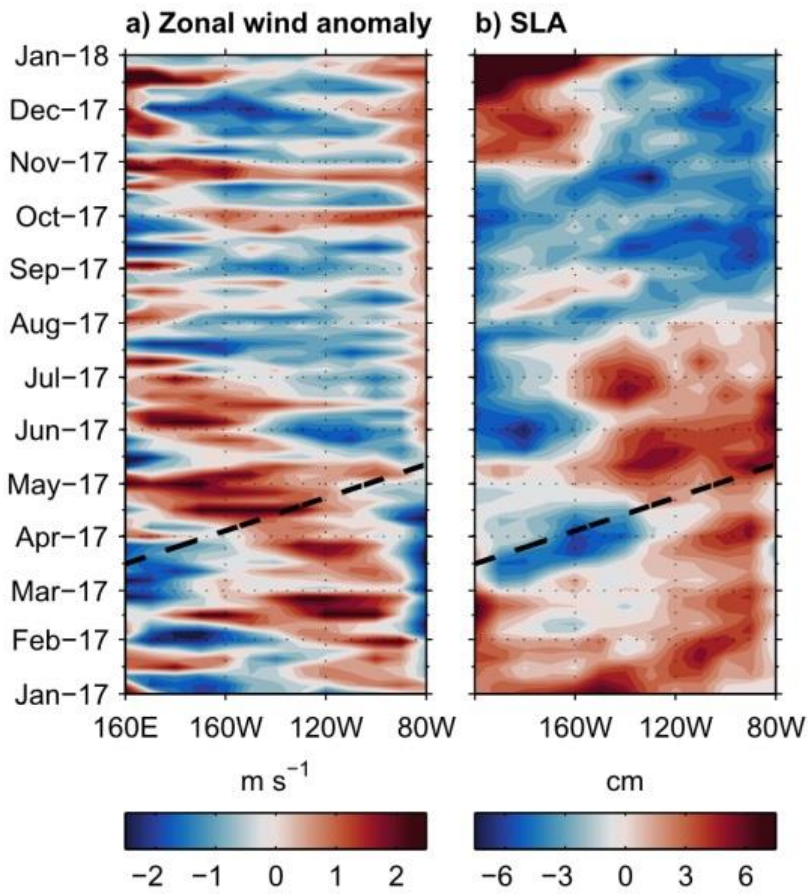
Figure 6: Hovmöller diagram of zonal wind anomaly (left panel) and SLA (right panel) along the central and eastern equatorial Pacific for the year 2017. The propagation of a first mode equatorial Kelvin wave is indicated by the dashed black line (phase speed 2.7 m s⁻¹; Yu and McPhaden, 1999).
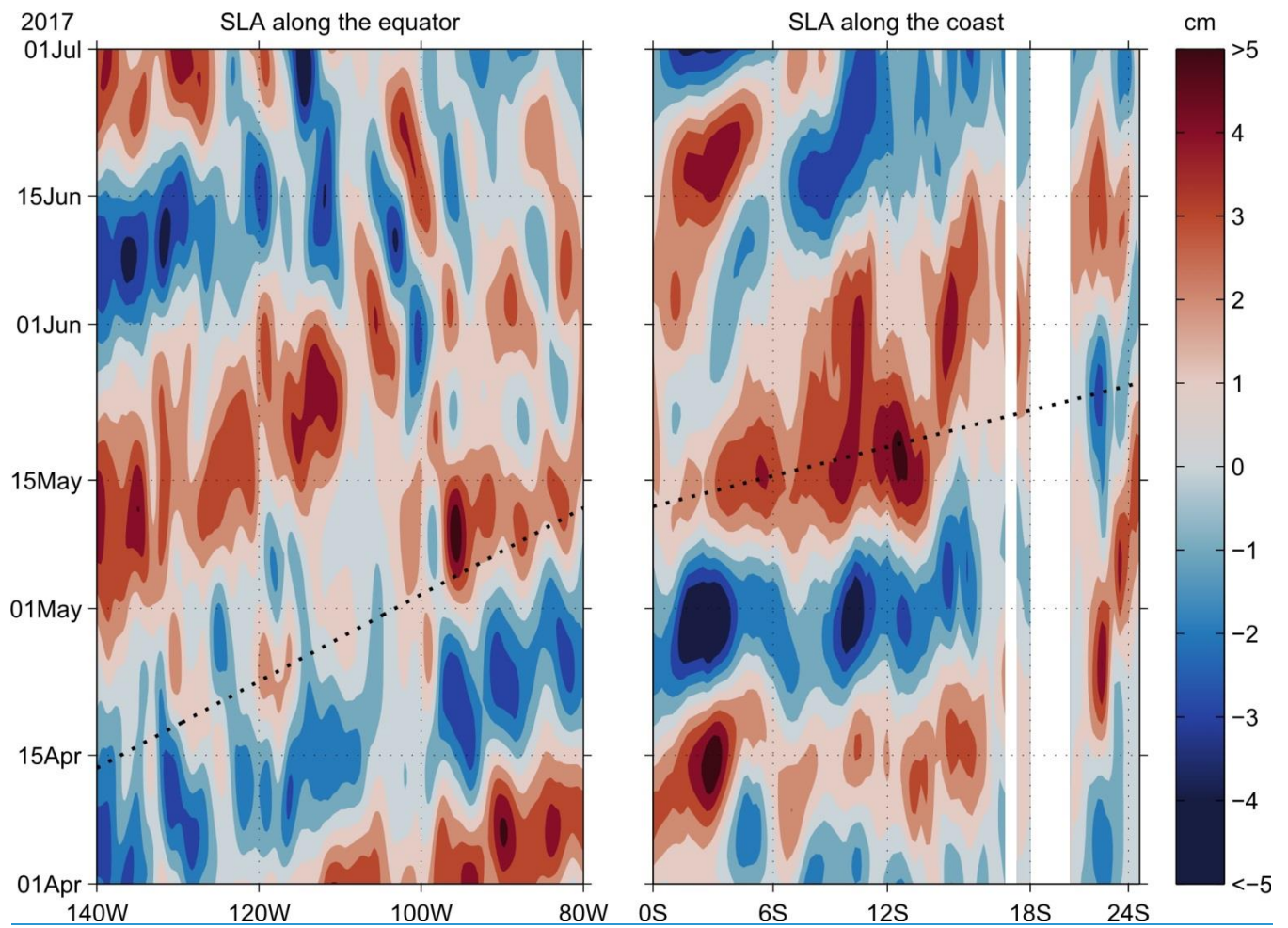
Figure 7
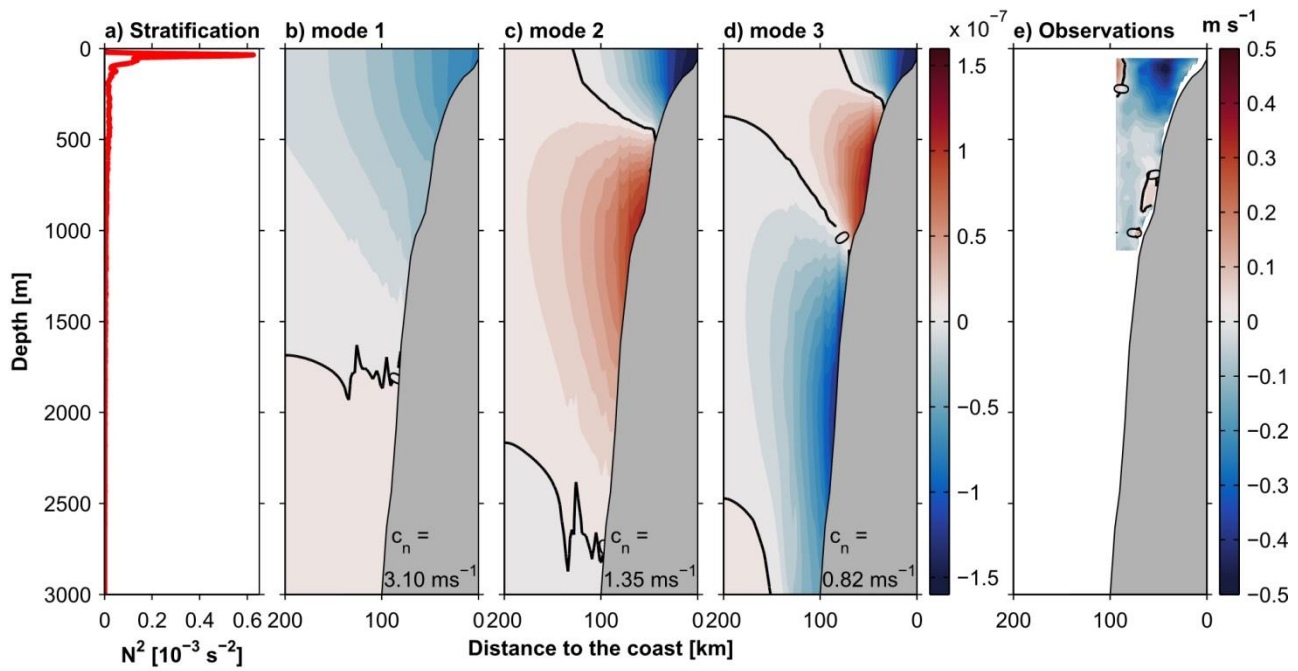
Figure 7: Profile of stratification (N²) (left panel) and cross-shore-depth structure of alongshore velocity (arbitrary amplitude) obtained for the first three CTW modes (panel b through d). Panel e) shows the difference of observed alongshore velocity between April 18 – May 03 and May 12 – 26, 2017. Note that the CTW phase speeds c_n are given in the lower right corner of the respective velocity structure panel.
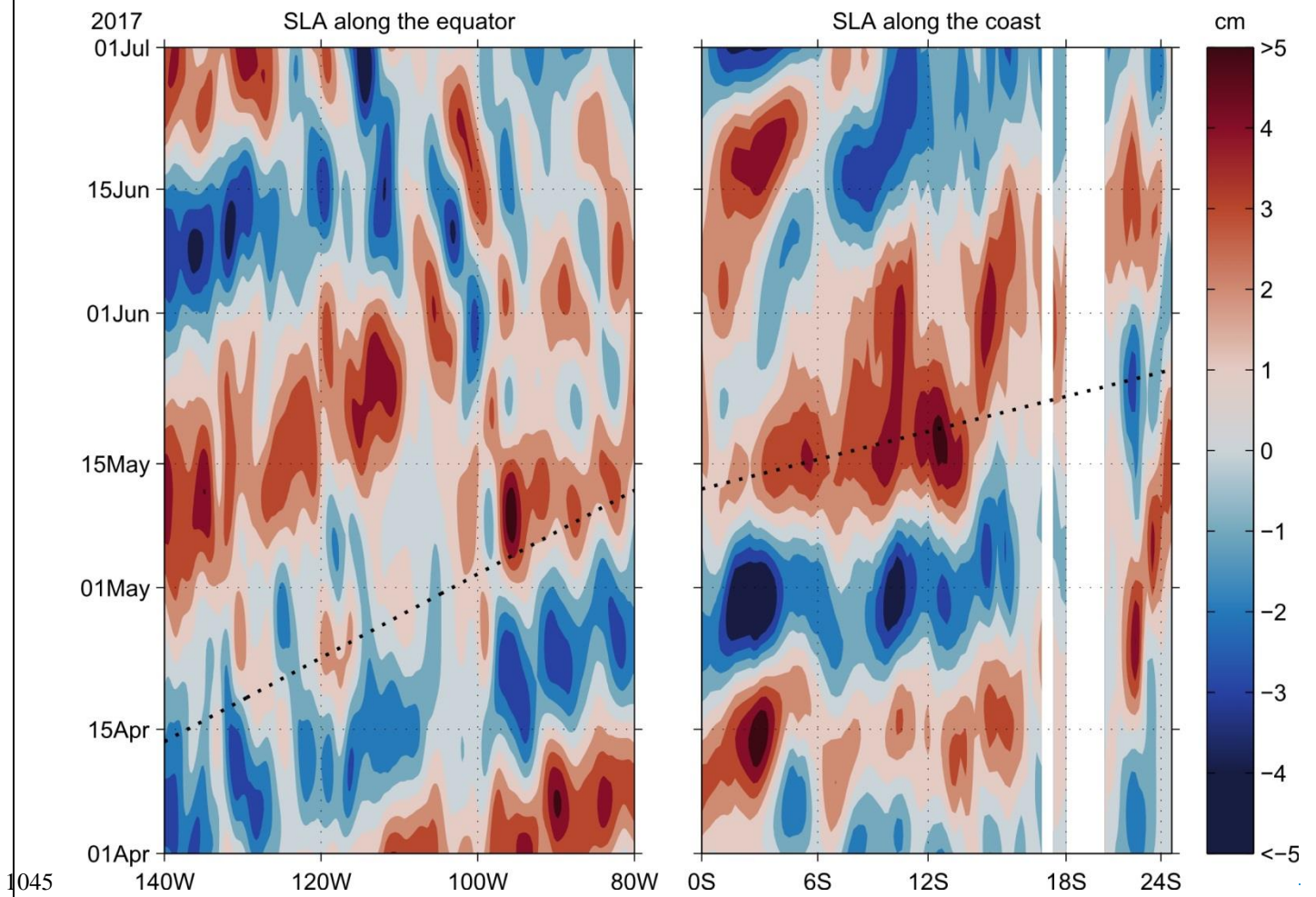
Figure 8: Bandpass filtered (20 – 90 days) sea level anomaly along the eastern equatorial Pacific averaged between 0.25°N and 0.25°S (left panel) and along the western coast of South America (right panel) averaged over the two grid point closest to the coastline. The propagation of a first mode equatorial Kelvin wave and CTW are shown as dotted black lines, phase speed of the equatorial wave is 2.7 m s⁻¹ (Yu and McPhaden, 1999) and 3.1 m s⁻¹ for CTWs (see figure 7b8b).
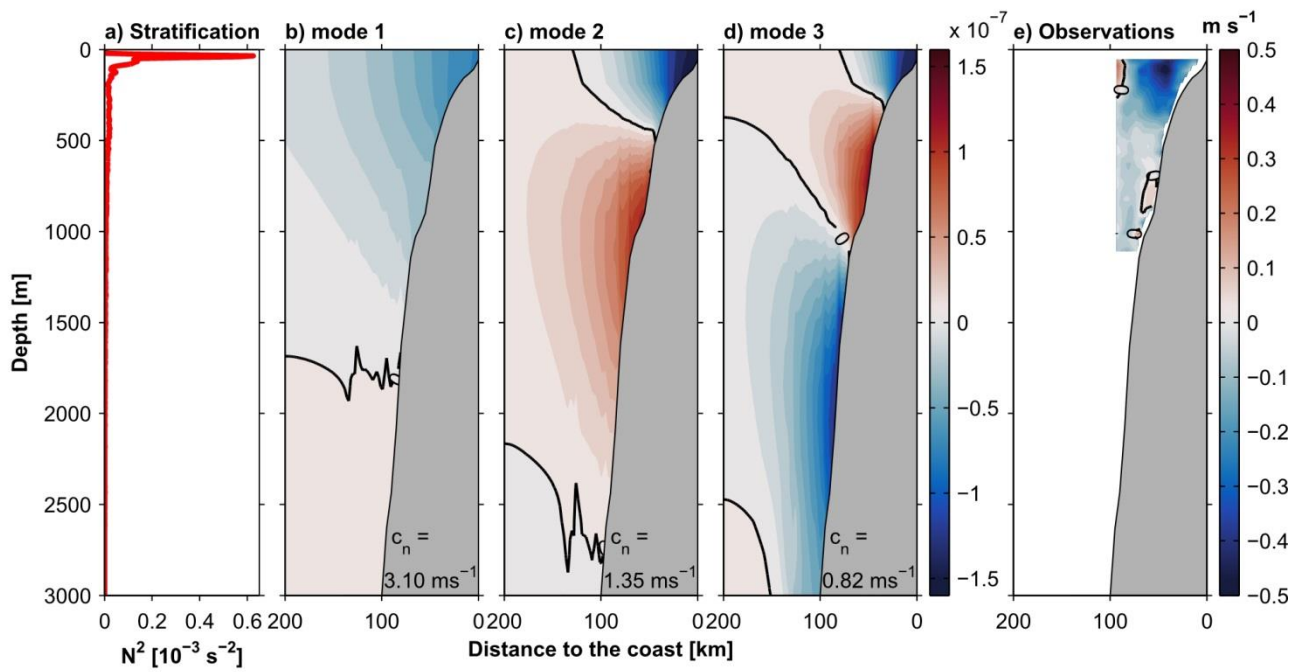
Figure 8: Profile of stratification (N^2) (left panel) and cross-shore-depth structure of alongshore velocity (arbitrary amplitude) obtained for the first three CTW modes (panel b through d). Panel e) shows the difference of observed alongshore velocity between April 18 – May 03 and May 12 – 26, 2017. Note that the CTW phase speeds c_n are given in the lower right corner of the respective velocity structure panel.
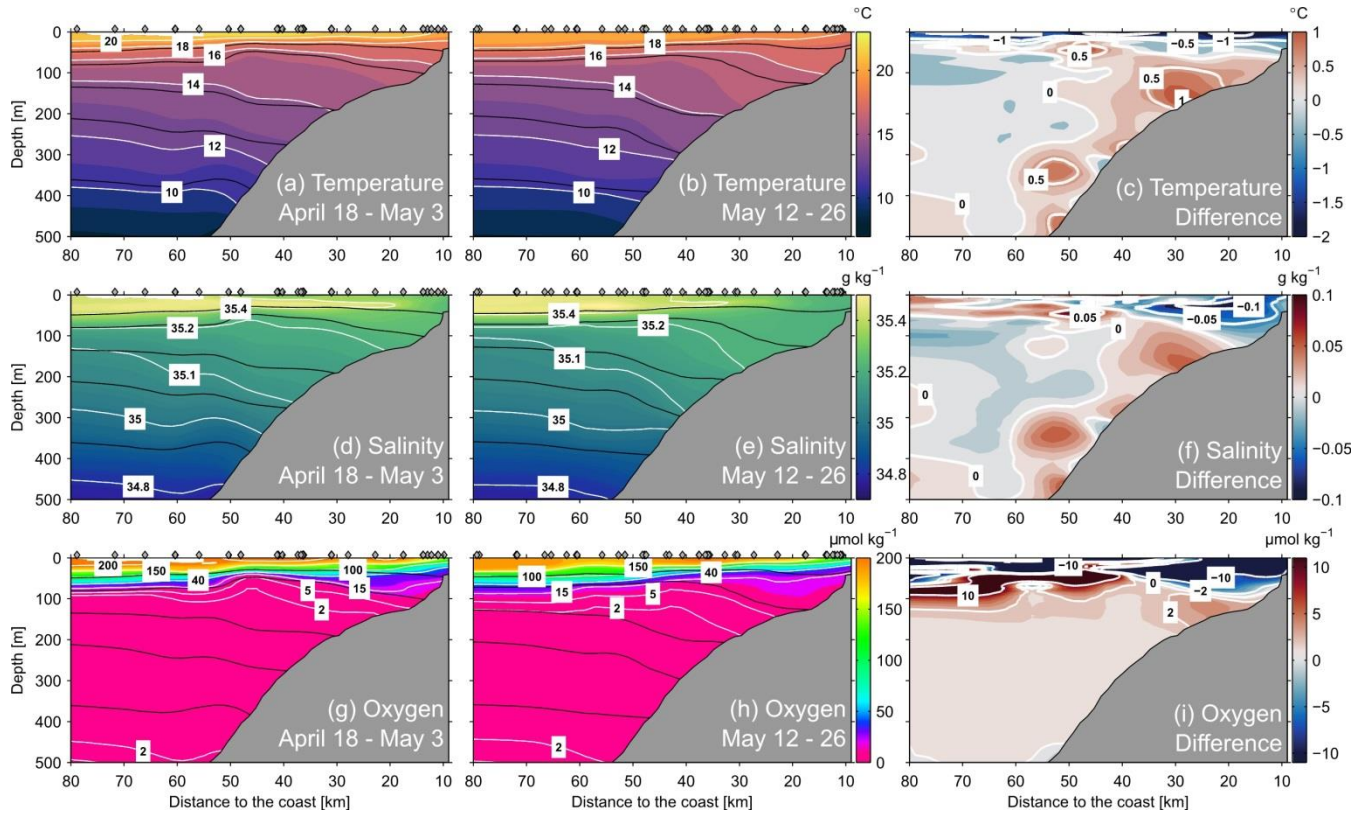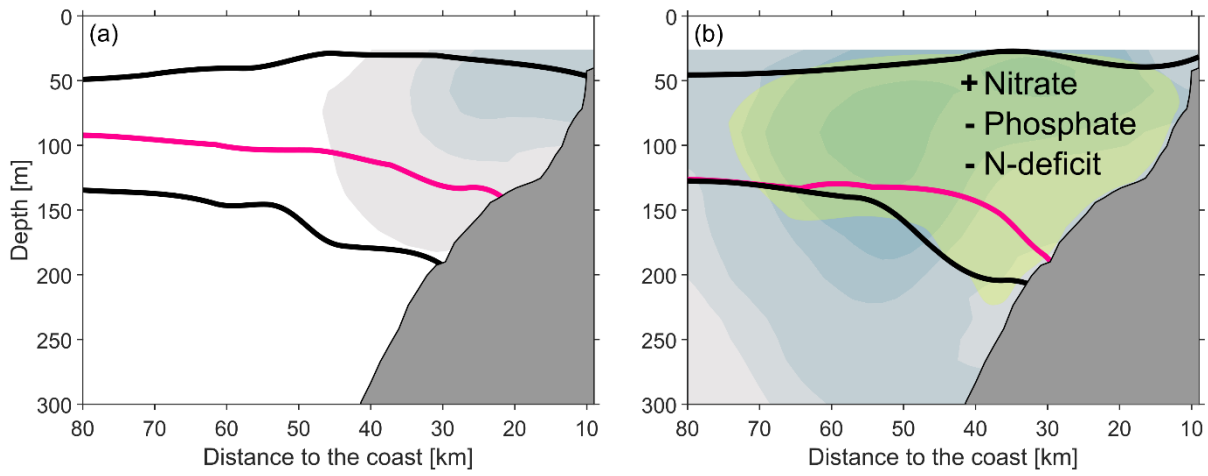
Figure 9: Conservative ~~Temperature~~temperature (upper panel row), absolute salinity (middle panel row), and oxygen (lower panel row) at 12° S during April 18 – May 3, 2017 (left panel column) and May 12 – 26, 2017 (middle panel column). The difference of the respective characteristic between the two periods is indicated in the right panels. Black lines indicate the distribution of isopycnals (σ_θ) 25.6, 25.9, 26.2, 26.4, and 26.7 kg m^{-3}. Grey diamonds mark positions of CTD stations.
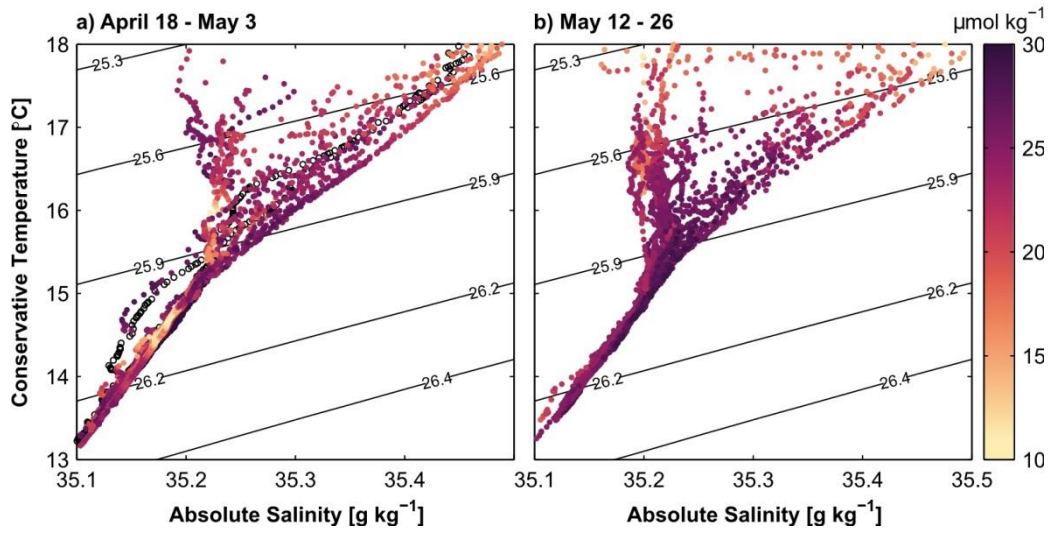
Figure 10: Conservative temperature – absolute salinity diagram between 50 and 300 m depth for CTD profiles between the 100 and 400 m isobaths during April 18 – May 3, 2017 (left panel) and May 12 – 26, 2017 (right panel). Colour code depicts nitrate concentrations. Black contours indicate isopycnals (σ_θ) in kg m^{-3}.
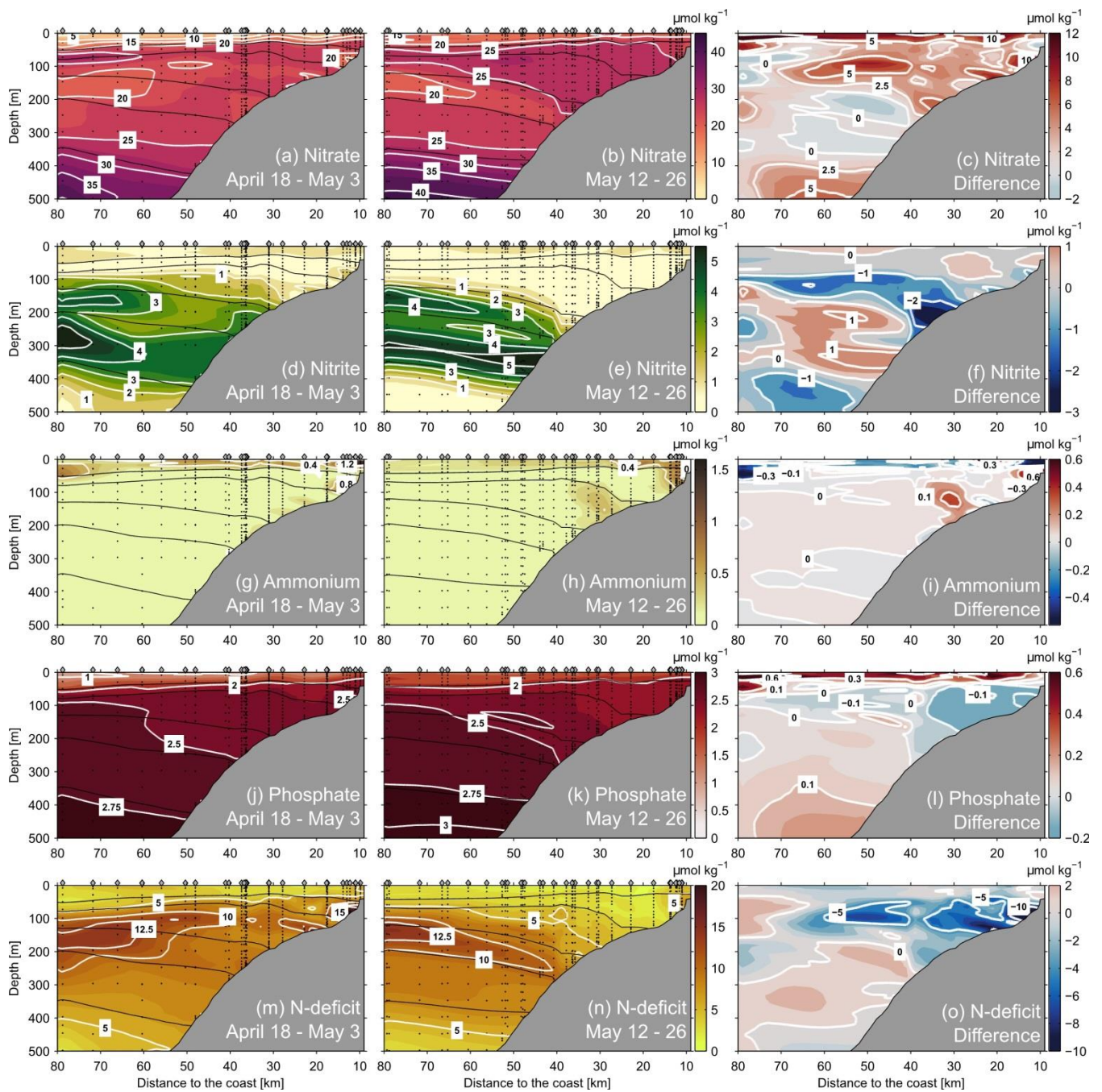
Figure 11: Nitrate (upper panels), nitrite (2nd panel row), ammonium (3rd panel row), phosphate (4th panel row) concentrations, and nitrogen deficit (bottom panel row) at 12° S during April 18 – May 3, 2017 (left panels) and May 12 – May 26, 2017 (middle panels). Concentration difference of the respective parameters between the two time periods are shown in the left panels. Black lines indicate the distribution of isopycnals (σ_θ) the 25.6, 25.9, 26.2, 26.4, and 26.7 kg m^{-3}. Grey diamonds mark the positions of CTD stations while black circles mark the position of bottle samples in the water column.

37

Figure 12: Schematic of the conditions off Peru during the initial phase of weak PCUC flow (a) and strong PCUC flow (b). Alongshore circulation is shown as colour shading, two isopycnals are sown in black and the top of the anoxic zone in magenta (represented by the 2 µmol kg^{-1} isoline). The green shaded area in (b) shows the region of increased nitrate, decreased phosphate concentrations and decreased nitrogen deficit.